UNIVERSIDAD DE CHILE
FACULTAD DE CIENCIAS FÍSICAS Y MATEMÁTICAS
DEPARTAMENTO DE INGENIERÍA CIVIL

INTEGRATED SURFACE-SUBSURFACE HYDROLOGIC MODELING TO QUANTIFY GROUNDWATER RECHARGE DUE TO AN EXTREME FLOODING EVENT IN THE ATACAMA DESERT

TESIS PARA OPTAR AL GRADO DE
MAGÍSTER EN CIENCIAS DE LA INGENIERÍA, MENCIÓN RECURSOS Y MEDIO AMBIENTE HÍDRICO

MEMORIA PARA OPTAR AL TÍTULO DE INGENIERO CIVIL

CRISTIAN EDUARDO PINO COLL

PROFESOR GUÍA:
PAULO HERRERA RICCI

MIEMBROS DE LA COMISIÓN:
JAMES MCPHEE TORRES
RENÉ THERRIEN

SANTIAGO DE CHILE
2018

SUMMARY OF THE THESIS SUBMITTED IN PARTIAL FULFILLMENT OF THE REQUIREMENTS FOR THE DEGREE OF CIVIL ENGINEER AND MASTER DEGREE IN ENGINEERING SCIENCES, MENTION IN WATER RESOURCES AND ENVIRONMENT.
BY: CRISTIAN EDUARDO PINO COLL
DATE: JULY 2018
THESIS ADVISOR: PAULO HERRERA RICCI

INTEGRATED SURFACE-SUBSURFACE HYDROLOGIC MODELING TO QUANTIFY GROUNDWATER RECHARGE DUE TO AN EXTREME FLOODING EVENT IN THE ATACAMA DESERT

Recharge of alluvial aquifers in arid regions mostly occurs during extreme flooding events, which are interspersed by long dry periods. Understanding the interactions between surface and ground water during and after such events is crucial to estimate recharge rates, which are needed to design systems and/or management strategies to optimize the use of the limited water resources of those areas. However, challenges remain to directly measure parameters that control infiltration in arid areas, such as fluctuations in surface flow depth and velocity, soil unsaturated flow properties and moisture conditions, and the hydraulic gradient at the surface-subsurface interface. Moreover, the thickness of the vadose zone is typically large in arid environments and there can be a very long delay between the flood event that generates the infiltration and the recharge of the aquifer, which complicates recharge estimations. These challenges motivated the application of an integrated surface and subsurface hydrologic model in an arid watershed to simulate recharge mechanisms during and after an extreme flooding event that occurred in an alluvial valley in Northern Chile. The model was calibrated to reproduce general trends in groundwater levels and surface flow discharges, providing a physically plausible representation of the spatial and temporal fluctuations of infiltration and recharge, which is estimated equal to 41 % of the flood volume. The calibrated model was then used to investigate the magnitude and spatio-temporal distribution of recharge and the response of the hydrologic system to different surface and subsurface parameters and initial conditions. Thus, the model allowed to investigate and identify mechanisms that control recharge and discuss potential improvements to apply this type of models to similar areas elsewhere.

RESUMEN DE LA TESIS PARA OPTAR AL TÍTULO DE INGENIERO CIVIL Y GRADO DE MAGÍSTER EN CIENCIAS DE LA INGENIERÍA, MENCIÓN RECURSOS Y MEDIO AMBIENTE HÍDRICOS.
POR: CRISTIAN EDUARDO PINO COLL
FECHA: JULIO 2018
PROF. GUÍA: PAULO HERRERA RICCI

MODELACIÓN HIDROLÓGICA INTEGRADA DE FLUJO SUPERFICIAL-SUBSUPERFICIAL PARA CUANTIFICAR LA RECARGA DE AGUAS SUBTERRÁNEAS DEBIDA A UN EVENTO EXTREMO DE INUNDACIÓN EN EL DESIERTO DE ATACAMA

En regiones áridas el agua subterránea constituye la principal fuente de agua para distintos usos. Teniendo en cuenta que la recarga principal de los acuíferos aluviales se origina durante eventos esporádicos de inundación que pueden ocurrir cada periodos secos prolongados sin ninguna recarga, es importante comprender la interacción entre el agua superficial y subterránea durante y después de dichos eventos para evaluar las tasas de recarga, gestionar y planificar de forma óptima el uso de los limitados recursos hídricos. La infiltración está controlada temporal y espacialmente por las fluctuaciones de la altura de escurrimiento, que junto a las propiedades de retención y condición de humedad del suelo determinan el gradiente hidráulico en la interface agua-sedimento y el volumen disponible para recargar. Por otro lado, en zonas áridas el espesor de la zona no saturada es típicamente grande, por lo que puede pasar un tiempo largo entre que ocurre la infiltración y se recarga el acuífero. Hoy en día, la medición in-situ de estos factores y la estimación espacio temporal de la recarga siguen siendo un desafío. Esto motiva la aplicación de un modelo totalmente acoplado de flujo superficial-subsuperficial basado en procesos físicos para estudiar los mecanismos de recarga durante y después de un evento extremo de inundación registrado en un valle aluvial del norte de Chile. El modelo calibrado para reproducir la tendencia general de los niveles de agua subterránea y caudal superficial observado permite investigar la magnitud y distribución temporal y espacial de la recarga del sistema, la cual se estimó en un 41 % del volumen de la crecida. Considerando diferentes parámetros superficiales y subterráneos, y diferentes condiciones iniciales de saturación se identifican variables y mecanismos que controlan la recarga originada por eventos extremos de inundación en el valle, y se extiende la discusión para mejoras en la aplicación de este tipo de modelos en sistemas hidrológicos similares, los cuales son comunes a otras regiones áridas del mundo.

Agradecimientos

Gracias a mi Familia y Amigos. Gracias a todos los que han dado Vida al Departamento de Ingeniería Civil Hidráulica. A los Profesores, Funcionarios y Alumnos. Gracias a la Universidad. A los que dedican su tiempo a los estudiantes y la Educación. Gracias a todos los que brindaron su tiempo y apoyo para el desarrollo de esta tesis. Gracias al Agua, a La Vida.

Tabla de Contenido

Introducción **1**
Motivación . . . 1
Caso de Estudio . . . 1
Objetivos . . . 2

Marco Teórico **4**
Proceso de Recarga . . . 4
Enfoque de modelación . . . 5

Cuerpo **11**
Introduction . . . 12
Numerical Model . . . 14
Study Area . . . 14
Model Setup . . . 16
Sensitivity Analysis . . . 18
Simulation Results . . . 20
Calibration . . . 20
Base Scenario . . . 23
Sensitivity Analysis . . . 27
Discussion and Conclusions . . . 36

Conclusiones **42**

Bibliografía **45**

Índice de Tablas

1. Subsurface parameter scenarios for sensitivity analysis. 19
2. Surface parameter scenarios for sensitivity analysis. 19
3. Calibrated subsurface parameters. Saturated hydraulic conductivity (K_s), specific storage (S_s), van Genuchten parameters (α and β) and residual and saturated volumetric water content (θ_r and θ_s, respectively). 21
4. Calibrated surface parameters. Manning's roughness coefficients (n_x and n_y), rill storage height (h_r), obstruction storage height (h_o). 21
5. Global model performance statistics for the calibrated base scenario. MAE: Mean absolute error, ME: Mean error, $RMSE$: Root mean square error, $NRMSE$: Normalized root mean square error, NSE: Nash–Sutcliffe coefficient for surface flow discharge. ΔO is the range of observed groundwater levels, O_i and S_i are observed and simulated values, $\overline{O}$ is the mean observed value and N is the number of observations. 22

Índice de Ilustraciones

1. Área de estudio y dominio del modelo. 3
1. Location of monitoring wells used for model calibration along the San José River valley (top). Mean monthly rainfall and depth to water table observed at monitoring wells (bottom - left) and 2001 observed flow discharge measured at Saucache station and the calibrated flood hydrograph set as a transient surface nodal flux boundary condition at the center of the eastern model boundary (bottom - right). 15
2. Spatial distribution of the homogeneous subsurface zones (top) and homogeneous surface zones (bottom). 17
3. Observed (circles) and simulated (solid lines) groundwater levels at selected monitoring wells. 23
4. Total infiltration and total flooded area delimitation. Colors represent the magnitude of the cumulative flood infiltration at flooded areas. 24
5. Temporal evolution of simulated infiltration rates and groundwater table depth (GWT) for the entire simulation at distances of 3, 12 and 29 km from the coast along the river axis. 24
6. Calibrated flood hydrograph (Q_C), total infiltration rate (inf) and simulated surface flow discharge (Q_s) (left); temporal evolution of surface water depth, depth of the inverted water table (IGWT), infiltration rate, and saturated hydraulic conductivity along the river axis (from left to right, respectively). . 25
7. Subsurface saturation at different simulation times for a vertical cross-section located under the river axis. A physical distortion exists because elevations are projected horizontally in a 2D rectangular plane. Note that the vertical axis representing the distance along the river is in kilometers, while the horizontal axis that shows depth under the river bed is in meters. 26
8. Difference between the final and initial groundwater levels, corresponding to the total simulated groundwater level rise. 27
9. Differences (residuals) between groundwater levels simulated at each well for the base scenario and levels simulated for the other scenarios. 28
10. Differences (residuals) between the simulated surface flow discharge at the Saucache gauging station for the base scenario and discharge simulated for the other scenarios. 29
11. Volume of infiltrated water and effective recharge for the final simulated time expressed as a percentage of the total flood volume for each simulated scenario. 30
12. Spatial distribution of total infiltration and flooded areas for the scenarios with greatest variations (K1, K6, P3 and N2). 31
13. Calibrated flood hydrograph (Q_C), total infiltration rate (inf) and simulated surface flow discharge (Q_s) (left panels); and temporal evolution of surface water depth, depth of the inverted water table (IGWT), infiltration rate, and saturated hydraulic conductivity along the river axis (from left to right, respectively) for scenarios K1, K6, P3 and N2 (from top to bottom). 32

14. Time of connection between surface and groundwater systems along the river axis for scenarios with maximum and minimum initial water table depth and for the base scenario [left]. Total infiltration and effective recharge as percentage of the total flood for different initial water table depth using the 24 layers vertical discretization for the based scenario (red circles) and a finer discretization (36 layers) (green triangles) [right]. 34
15. Temporal distributions of the flood volume in 4 pulses of 20 days and the resulting simulated infiltration. Pulses are released (δ_p) every 20 (no lag between pulses), 50, 100, 200 and 400 days. 35
16. Vertical saturation profiles under the river bed just before the second pulse for the different temporal distributions of the total flood volume shown in Fig 15 [left]; and total recharge as percentage of the total flood volume for the different temporal distributions [right]. 36
S1. Groundwater table depth along the river longitudinal profile during the simulated time interval. 40
S2. Infiltration rates during flooding event and GWT depth for the entire simulation at 3, 12 and 29 km from the coast along the longitudinal river profile of Fig4 , for the scenarios K1, K6, P3 and N2. 41

Introducción

Motivación

Las aguas subterráneas son un recurso esencial para el ser humano y el medio ambiente. La correcta evaluación y medición de la variabilidad espacio-temporal de la recarga natural de los acuíferos y su modificación debida a acciones antrópicas comprende uno de los principales desafíos para el ser humano para asegurar una gestión y planificación racional de los recursos hídricos. A pesar que los procesos y mecanismos de recarga son relativamente bien conocidos, la incertidumbre en su estimación, a veces cuantificable, acotable y en casos extremos difícil de estimar, usualmente no se reconoce ni comprende de forma explícita. Hoy en día, esta incertidumbre en la estimación de los recursos subterráneos, y también de los demás componentes del ciclo hidrológico, asociada en primera instancia a la inherente variabilidad climática a sus distintas escalas temporales y espaciales, no impide: observar, medir, conocer y caracterizar el recurso y los procesos físicos que rigen su comportamiento. La incertidumbre relativa a la variabilidad espacial de los factores que determinan la ocurrencia, magnitud y calidad de la recarga, se puede evaluar y reducir mediante la utilización de distintos métodos y herramientas complementarias. Una mejora progresiva de la gestión y planificación requiere del avance conjunto en la observación, calibración de los métodos de estimación y la investigación de procesos (Custodio et al., 1997).

En particular, en Chile un efecto combinado de un aumento en las temperaturas y cambios en los patrones de precipitación (Garreaud, 2011), y una intensificación de las condiciones de aridez y semi aridez hacia el centro y sur del país (Valdés-Pineda et al., 2014), junto al aumento de la población y expansión de las ciudades, pone al país frente a un escenario crítico en torno a los recursos hídricos (Andrew Maddocks and Paul Reig, 2015). Para mejorar la capacidad de planificación y gestión del agua, asegurar su disponibilidad, calidad, y prevenir los daños asociados a eventos extremos, se vuelve de suma importancia estudiar y caracterizar los sistemas de agua subterránea, en particular en las zonas áridas y semi-áridas del país, la dinámica de su recarga-descarga y su relación con las aguas superficiales.

Caso de estudio

En el Desierto de Atacama, uno de los lugares más áridos del mundo, la precipitación media anual es del orden de los 10 mm, el agua superficial es escasa y los ríos son en su mayoría efímeros. A pesar de estas condiciones de aridez extrema, importantes ciudades se han desarrollado en los valles inferiores y la depresión central, donde los acuíferos, en su mayoría sobreexplotados, constituyen la principal fuente de agua para distintos usos. El agua que recarga estos acuíferos tiene su origen sobre los 3500 msnm, en la alta cordillera y el altiplano, donde existe un clima tropical con lluvias intensas durante los meses de verano (diciembre - marzo) (Houston, 2006b). Cada ciertos años durante estos eventos de precipitación de alta intensidad, la capacidad de infiltración de los suelos es con creces superada y grandes flujos superficiales escurren por valles y quebradas, recargando los acuíferos aluviales y fluviales, a

la vez que producen importantes daños a la vida humana, la economía e infraestructura (p.ej. Arica 1973, Atacama 2001 y 2009, Copiapó 2012, Antofagasta 2016 y 2017, entre otros).

En el Valle de Azapa, ubicado al norte del Desierto de Atacama, existen condiciones climáticas que han permitido el cultivo de hortalizas durante todo el año, convirtiéndolo en el principal abastecedor del país durante el invierno. Con aproximadamente 3000 ha cultivadas, la agricultura del valle representa un 30 % de la economía regional. Debido a un incremento sostenido de la productividad agrícola durante los últimos 40 años, con el consiguiente aumento de la demanda de agua para irrigación, el acuífero de Azapa se encuentra sobreexplotado. El descenso de los niveles piezométricos en el valle ha reducido la eficiencia de las bombas de extracción, ha obligado a la profundización de pozos, reducido el afloramiento de vertientes, y empeorado la calidad del agua por salinización (H. Peña, 1995). La precipitación media anual en el Valle de Azapa no sobrepasa los 3 mm, sin embargo, en la parte alta de la cuenca del rio San José (sobre los 2000 msnm), el cual se extiende de este a oeste a lo largo del Valle de Azapa, la precipitación media anual, concentrada sobre todo entre diciembre y marzo, puede sobrepasar los 400 mm. Así, el rio San José corresponde a un río efímero que en los meses estivales del Invierno Altiplánico logra alcanzar su curso inferior y desemboca en el mar. Estos eventos esporádicos de inundación constituyen la principal recarga del acuífero de Azapa (Taylor, 1949; JICA, 1995; H. Peña, 1995; Arrau, 1997; AC, 2010; Jiménez Martínez, 2013; INH, 2014), a la vez que producen perdidas de suelos productivos y sus cultivos, en infraestructura, vida humana y animal.

Objetivos

El objetivo principal de esta tesis es la aplicación de un modelo totalmente acoplado para simular flujo superficial-subterráneo para estudiar la recarga por infiltración durante eventos extremos de inundación en el acuífero fluvio-aluvial del Valle de Azapa (Fig 1).

Objetivos específicos:

- Desarrollar un modelo tridimensional del acuífero de Azapa en Hydrogeosphere (Therrien et al., 2010; Brunner and Simmons, 2012; Aquanty Inc, 2013).
- Utilizar el modelo para identificar e investigar mecanismos que controlen espacial y temporalmente la recarga, evaluando la sensibilidad del modelo a variaciones en los parámetros y condiciones que lo definen.
- Evaluar la aplicabilidad de este tipo de modelos para el estudio de la recarga subterránea en zonas áridas.

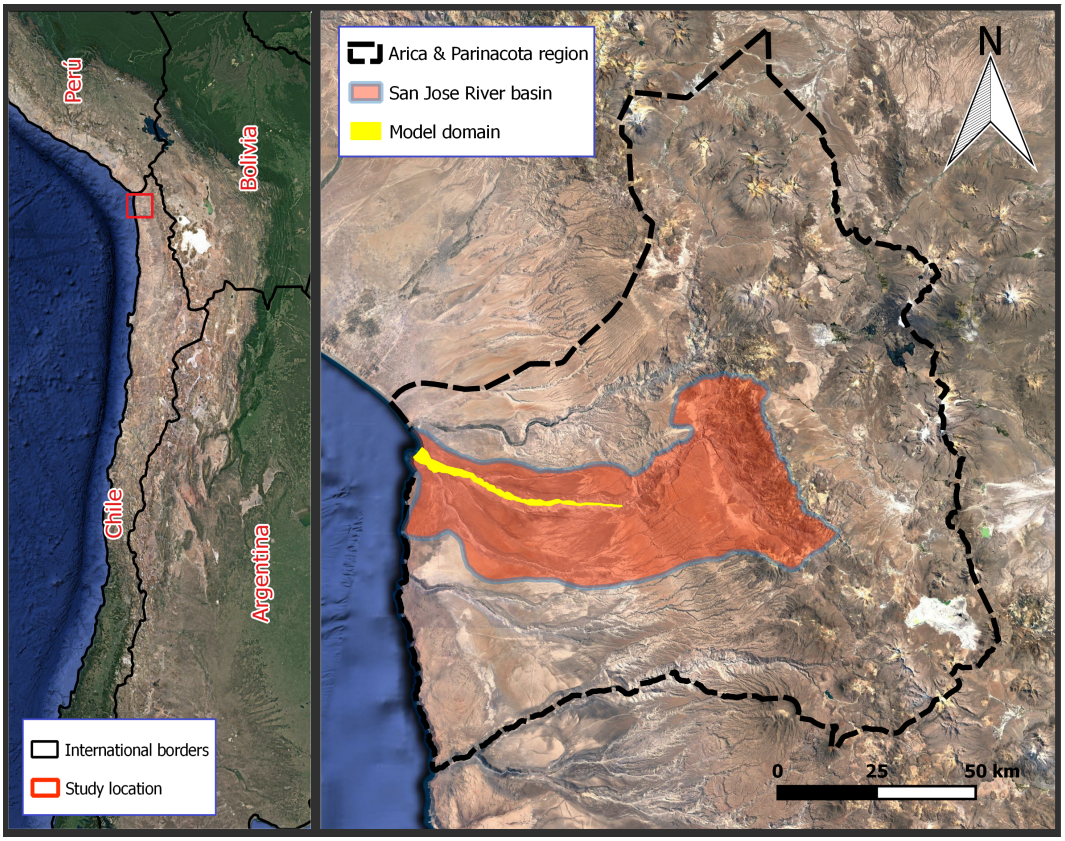

Figure 1: Área de estudio y dominio del modelo.

Marco Teórico

Proceso de recarga

La recarga corresponde al proceso de incorporación de agua a un acuífero. Esta puede ocurrir principalmente por infiltración de lluvia, aguas superficiales o transferencia de agua desde otro acuífero. El clima limitará los potenciales flujos de entrada a la superficie y el subsuelo. Diferentes factores como el relieve, la topografía a diferentes escalas, desde kilómetros a centímetros, y el uso del suelo, controlan el progreso, magnitud y redistribución del agua superficial disponible para infiltrar. Entre el agua superficial y subterránea se establece una continuidad hidráulica a través del contenido de humedad en el suelo. A pesar de que este generalmente constituye una fracción pequeña del balance hídrico, cumple un rol fundamental de memoria de condiciones previas de sequía o humedad que tienden a persistir y controlar eventos futuros del ciclo hidrológico a distintas escalas (Koster and Suarez, 2001; Western et al., 2002).La humedad del suelo determina de una manera no lineal la transitoriedad en el almacenamiento, las variaciones en la escorrentía, la evapotranspiración y el intercambio energético con la atmósfera. Así, la infiltración dependerá del gradiente hidráulico en la interfaz agua sedimento y la permeabilidad de estos. La cantidad de agua que llega al nivel freático y constituye la recarga dependerá principalmente de: a) la extracción de las raíces en las primeras capas del suelo y la evaporación, b) la estructura del suelo, la cual determina su porosidad y permeabilidad intrínseca, que a su vez depende del contenido de humedad del suelo, y c) la profundidad del nivel freático, la cual junto a la estructura del suelo y contenido de humedad en la zona no saturada definen el volumen disponible para recargar. (Sorman and Abdulrazzak, 1993; Sophocleous, 2002; Bethune et al., 2008; Doble et al., 2011).

Mientras existe infiltración puede ocurrir un estado de conexión o desconexión hidráulica entre agua superficial y subterránea cuando el nivel de agua superficial es superior al nivel freático. Una continuidad del medio saturado entre el agua superficial y el acuífero da lugar a un estado de conexión hidráulica en que la infiltración dependerá de la permeabilidad de los sedimentos y el gradiente hidráulico. Por otro lado, si debajo del curso superficial el medio se encuentra parcialmente saturado, se produce un estado de desconexión hidráulica, pudiendo: a) ocurrir un descenso vertical de un frente de saturación que se aproxima al nivel freático y generará una situación de conexión hidráulica al alcanzarlo, con la consecuente recarga del acuífero, o b) la mantención de una zona no saturada bajo el cauce con transferencia de agua hacia el nivel freático produciéndose la recarga (p.ej. si existe una capa de menor permeabilidad en el lecho del cauce, o para pequeñas profundidades de agua y ancho del cauce, y niveles freáticos profundos) (Bouwer, 2002; Brunner et al., 2009a; Xie et al., 2014). Para mantener este medio no saturado el agua infiltrada debe transferirse por el acuífero a otras áreas, sino el agua se acumula bajo el área de recarga y el nivel freático puede llegar a conectarse hidráulicamente con el cuerpo de agua superficial.

En general la recarga es variable y discontinua en el tiempo, lo que se traduce en elevaciones transitorias del nivel freático. Existe una distinción temporal y de magnitud entre infiltración y recarga, debido a la transferencia de agua por la zona no saturada. Para una recarga media

R [L/T], el tiempo de transito medio del agua en un espesor H [L] de suelo no saturado y contenido medio volumétrico de humedad θ, puede expresarse como τ=Hθ/R [T]. Así el agua que infiltra en superficie en un tiempo determinado no es la que produce la respuesta en el nivel freático, sino la que infiltró hace un tiempo τ, el cual puede variar entre horas y cientos de días. Este efecto es de particular interés en zonas áridas, donde el nivel freático se encuentra en general profundo, generándose una situación de conexión y desconexión entre los efímeros cursos superficiales y los acuíferos, y una redistribución del agua infiltrada en la zona no saturada. Esto sumado a las características extremas y esporádicas de los flujos superficiales que recargan estos acuíferos, dificulta la estimación y medición fiable de la recarga en estas zonas.

Enfoque de modelación

La modelación numérica integrada de sistemas hidrológicos basada en relaciones físicas, tales como conservación de masa, momentum y energía, avanza en resolver la interacción entre los componentes hidrológicos atmosféricos, superficiales y subterráneos, y la dinámica de la humedad a sus distintas escalas temporales y espaciales. Los avances en las tecnologías de la información y computación de alto rendimiento, en la adquisición y procesamiento de datos con enfoque en el estudio de las ciencias de la tierra, junto a la evaluación y mejora de los métodos numéricos, ha permitido evaluar y mejorar la compresión de los procesos hidrológicos de una manera integrada por medio de la aplicación concreta de diversos modelos basados en la física (Sellars et al., 2013; Maxwell et al., 2014; Bierkens et al., 2015; Paniconi and Putti, 2015; Fatichi et al., 2016; McCabe et al., 2017).

Este tipo de modelación constituye una útil herramienta para desarrollar conceptos, entender y caracterizar los principales procesos físicos y sus interacciones, ya que se incluyen en la formulación del modelo. Los modelos hidrológicos integrados de flujo superficial-subsuperficial (ISSHM) han permitido por ejemplo, reducir la incertidumbre asociada a la definición de las zonas y magnitudes de intercambio de masa y energía (p.ej. escorrentía, zonas de inundación y recarga y descarga subterránea, etc.), quedando determinadas por los parámetros con significado físico que caracterizan el medio (p.ej. topografía, microtopografía, características de los suelos, etc.) y las forzantes meteorológicas del sistema a una resolución y escala determinada, en lugar de ser un parámetro a calibrar. Esto permite contribuir a un mejor conocimiento de los fenómenos simulados, a la vez que se acota el rango posible de valores adoptados de los parámetros que describen el sistema a valores más representativos de las escalas simuladas.

Así, al considerar la inherente interrelación existente entre los distintos procesos naturales de flujo y transporte, estos modelos permiten sintetizar, correlacionar y evaluar la constante información que se adquiere de un sistema (atmosférica, con superficial, subterránea, con las plantas, minerales, etc), añadiendo valor a esta. Por medio de un proceso iterativo de actualización, de evaluación de la relevancia de los procesos modelados a sus distintas escalas (Blöschl and Sivapalan, 1995; Beven, 1995; Western et al., 2002) (lo que permite la cuantificación de los errores por simplificación) y utilizando observaciones de distinto tipo (Khu et al., 2008; Finger et al., 2011), se puede generar una herramienta robusta, capaz de reproducir los procesos hidrológicos naturales y su relación con el ser humano a diversos niveles de detalle,

mejorar la gestión inetraga del recurso, y anticipar y prevenir eventos anormales o extremos que escapan a ser comprendidos y caracterizados por modelos más simples. La parsimonia es conveniente, pero la complejidad es frecuentemente necesaria (Ebel and Loague, 2006; Fatichi et al., 2016; Guthke, 2017).

Si bien, la consideración de la interacción entre agua superficial y subterránea durante eventos de inundación en regiones áridas ha permitido por medio de modelos conceptuales y numéricos, estimar la recarga natural a los acuíferos, evaluar alternativas de recarga artificial y de pronóstico y alerta de crecidas, por ejemplo: utilizando herramientas de información geográfica e imágenes satelitales (Abdalla et al., 2014); mediciones de altura de agua y relaciones empíricas de precipitación escorrentía (Hassan, 2011); modelos unidimensionales de onda cinemática y relaciones empíricas de infiltración (Morin et al., 2009; Philipp and Grundmann, 2013); rastreo de crecidas basado en el método de Muskingum con incorporación de coeficientes de perdida por infiltración (Cools et al., 2012; Cheng et al., 2015; Elfeki et al., 2015); modelación semidistribuida basada en la física acoplando el método de onda cinemática para el rastreo de crecidas con la ecuación de Richards' en una dimensión para el flujo subterráneo (El-Hames and Richards, 1998); etc... hoy en día existe poca documentación sobre la aplicación de modelos hidrológicos integrados de flujo superficial-subsuperficial (ISSHM) para el estudio de la recarga en regiones áridas a la escala de cuenca.

En el presente trabajo se utiliza el modelo numérico Hydrogeosphere (Therrien et al., 2010; Brunner and Simmons, 2012; Aquanty Inc, 2013) para estudiar la interacción entre el agua de crecidas extremas del río San José y el agua subterránea del acuífero de Azapa. Hydrogeosphere resuelve de forma simultánea, y de una manera totalmente acoplada para cada paso de tiempo, los componentes principales del ciclo hidrológico, es decir, los regímenes e interacciones de flujo superficial, subsuperficial y subterráneo.

Para representar estos procesos el modelo se basa en la resolución de balances hídricos, los cuales en su forma más general, para cualquier masa de agua en cualquier intervalo de tiempo, pueden ser representados como se describen a continuación.

Balance de agua superficial:

$$P = (Q_{So} - Q_{S\mathrm{i}}) - Q_{GS} + ET_S + Q_S^W + \Delta S_S$$

Balance de agua subterránea:

$$I = (Q_{Go} - Q_{G\mathrm{i}}) + Q_{GS} + ET_G + Q_G^W + \Delta S_G$$

Suma de los balances superficial y subterráneo (Balance hidrológico total):

$$P = (Q_{So} - Q_{S\mathrm{i}}) + (Q_{Go} - Q_{G\mathrm{i}}) + (ET_S + ET_G) + (Q_S^W + Q_G^W) + (\Delta S_S + \Delta S_G)$$

donde

P: Precipitación.

$Q_{S\mathrm{i}}$ y Q_{So}: agua superficial que entra y sale del sistema.

Q_{GS}: interacción agua superficial-subsuperficial.

ET_S: evapotranspiración desde agua superficial.

Q_S^W: extracciones de agua superficial.

ΔS_S: almacenamiento de agua superficial.

Q_{Gi}, Q_{Go}: agua subterránea que entra y sale del sistema.

ET_G: evapotranspiración desde agua subsuperficial.

Q_S^W: extracciones de agua subterránea.

ΔS_G: almacenamiento de agua subterránea.

El sistema hidrológico integrado se resuelve simultáneamente resolviendo la ecuaciones integradas en la profundidad (2D) de Saint-Venant para modelar el flujo de agua superficial, y la ecuación 3D de Richards para el flujo variablemente saturado en el suelo.

La malla numérica 2D utilizada para resolver el flujo superficial, se extiende en la dirección vertical para generar una malla 3D para resolver las ecuaciones de flujo subterráneo. El acoplamiento completo de los regímenes superficial y subsuperficial se realiza para cada paso de tiempo en función de la hipótesis de continuidad de carga hidráulica entre la superficie y el dominio subsuperficial (Therrien and Sudicky, 1996) o sobre la base de un coeficiente de intercambio de primer orden (Park et al., 2009; Ebel et al., 2009). El modelo teórico de movimiento e intercambio de agua entre los componentes superficial y subterránea y sus relaciones constitutivas para fines de la presente tesis se resume a continuación.

Ecuación de onda difusiva para el flujo superficial (2D)

$-\nabla \cdot \mathrm{d}_o \overrightarrow{q_o} - \mathrm{d}_o \Gamma_o \pm Q_o = \frac{\partial \phi_o h_o}{\partial t}$

d_o: profundidad de agua superficial $[L]$.

Γ_o: flujo de intercambio con el dominio subterráneo $[L^3 L^{-3} T^{-1}]$.

Q_o: términos fuente (caudales, extracciones, etc) $[LT^{-1}]$.

ϕ_s: porosidad del dominio superficial [-].

$h_o = z_o + \mathrm{d}_o$: elevación de la superficie de agua superficial; (z_o: elevación del terreno) $[L]$.

$\overrightarrow{q_o} = -\frac{\mathrm{d}_o^{2/3}}{\overrightarrow{n}\overrightarrow{\Phi}^{1/2}} k_{ro} \nabla (\mathrm{d}_o + z_o)$: flujo superficial (ecuación de Manning 2D) $[LT^{-1}]$

$\overrightarrow{n}$: coeficiente de rugosidad de Manning $[L^{-1/3}T]$

$\overrightarrow{\Phi}$: gradiente del agua superficial [-]

k_{ro}: factor para considerar reducciones en la conductancia horizontal debido a obstrucciones en el almacenamiento superficial. [-]

Conceptualización de la microtopografía:

Se tienen en cuenta los efectos de almacenamiento superficial debido a la presencia de surcos, vegetación, edificios, etc. Las alturas de depresiones h_r y obstrucción de almacenamiento h_o son parámetros con significado físico que geométricamente representan el espacio vacío dentro de los respectivos elementos de almacenamiento como función de la altura de flujo. El área horizontal cubierta por agua superficial varía entre cero y el área total a medida que el nivel de agua se eleva por sobre la superficie de terreno (z_o, definido como el fondo de las depresiones) hasta la máxima elevación $z_o + h_r + h_o$. El escurrimiento superficial ocurre solo cuando la carga en los nodos es mayor a una elevación de $z_o + h_r$. Así, se afecta el término de conductancia a través del factor k_{ro}, el cual varía desde $z_o + h_r$ a $z_o + h_r + h_o$ dentro de la zona de obstrucción. Para mayor detalle ver Panday and Huyakorn (2004).

Ecuación de Richards para el flujo subsuperficial variablemente saturado (3D).

$-\nabla \cdot \omega_m \overrightarrow{q} + \Gamma_o \pm Q = \omega_m \frac{\partial \theta_s S_w}{\partial t}$

ω_m: fracción volumétrica del medio poroso [-].

Γ_o: flujo de intercambio con el dominio superficial $[L^3 L^{-3} T^{-1}]$.

Q: términos fuente (extracciones, recargas, etc) $[L^3 L^{-3} T^{-1}]$.

θ_s: porosidad [-]

S_w: saturación [-]

$\overrightarrow{q} = \overrightarrow{K} \cdot k_r \nabla (\psi + z)$: flujo subsuperficial $[LT^{-1}]$

$\overrightarrow{K}$: permeabilidad $[LT^{-1}]$

k_r: permeabilidad relativa [-]

ψ: altura de presión $[L]$

z: elevación $[L]$

Basado en Van Genuchten (1980):

$$S_w = \begin{cases} S_{wr} + (1 - S_{wr})[1 + |\alpha\psi|^{\beta}]^{-\nu} & cuando \;\; \psi < 0 \\ 1 & cuando \;\; \psi \geq 0 \end{cases}$$

S_{wr}: saturación residual [-]

y

$k_r = S_{\mathrm{e}}^{lp}[1 - (1 - S_{\mathrm{e}}^{1/\nu})^{\nu}]^2$

$S_{\mathrm{e}} = (S_w - S_{wr})/(1 - S_{wr})$

$\nu = 1 - 1/\beta$; con $\beta \; > \; 1$

α: inverso de la presión de entrada de aire $[L^{-1}]$.

β: índice de distribución del tamaño de poro [-].

l_p: parámetro de conectividad de poros, igual a 0.5 para la mayoría de los suelos (Mualem, 1976).

Acople superficial-subsuperficial

El esquema *dual node* es usado para representar simultáneamente el flujo en la superficie y el dominio subsuperficial. El término de intercambio está dado por:

$\mathrm{d}_o\Gamma_o = \frac{k_r K_{zz}}{l_{exch}} (h - h_o)$

h: altura (presión) de agua subsuperficial $[L]$.

l_{exch}: longitud de acople $[L]$ (Ebel et al., 2009).

Si Γ_o es positivo, el flujo ocurre desde la subsuperficie a la superficie y k_r es la permeabilidad relativa del medio poroso. Cuando el flujo de agua es de la superficie al subsuelo Γ_o es negativo y

$$k_r = \begin{cases} S_{exch}^{2(1-S_{exch})} & \text{cuando} \;\; \mathrm{d}_o < H_s \\ 1 & \text{cuando} \;\; \mathrm{d}_o > H_s \end{cases}$$

H_s: altura total de obstrucción $(h_r + h_o)$ $[L]$

$S_{exch} = \mathrm{d}_o/H_s$ [-]

Las ecuaciones de flujo superficial y subterráneo se discretizan empleando el método de volumen de control en elementos finitos (Letniowski and Forsyth, 1991). Puede utilizarse un procedimiento de solución con paso de tiempo variable de acuerdo al comportamiento transiente del sistema y la tasa de cambio de la solución, lo cual permite considerar grandes pasos de tiempo si la solución no experimenta cambios drásticos de las variables definidos por

el usuario. El conjunto de ecuaciones no-lineales discretas se linealiza utilizando la técnica de Newton-Raphson. HGS puede ser paralelizado utilizando la interfaz de programación de aplicaciones OpenMP.

HGS es capaz de representar otros procesos, tales como: evapotranspiración, derretimiento de nieve, transporte de solutos, fracturas discretas, medios de doble porosidad, pozos, canales, drenes, etc.; los cuales son descritos en detalle y ejemplos, junto a mayor información sobre la teoría de HGS y el modelo numérico, en el manual de usuario (Aquanty Inc, 2013).

Actualmente HGS no cuenta con una interfaz gráfica. El archivo de construcción del modelo corresponde a un documento de texto con la extensión .grok, donde debe programarse las distintas funciones y comandos de HGS, las cuales se presenta con detalle en el manual de usuario (Aquanty Inc, 2013). Los archivos de entrada al modelo, tales como malla, elevaciones, parametrización espacial, condiciones iniciales y de borde fueron trabajadas en SIG y MATLAB, al igual que para la visualización de los resultados.

Integrated surface-subsurface hydrologic modeling to quantify groundwater recharge due to an extreme flooding event in the Atacama Desert

C. Pino[1] R. Therrien[2] P. Herrera[1*]

[1] *Department of Civil Engineering, U. de Chile.*
[2] *Department of Geology and Geological Engineering, U. Laval.*
[1*] *Now at Robertson GeoConsultants Inc.*

Abstract

Recharge of alluvial aquifers in arid regions mostly occurs during extreme flooding events, which are interspersed by long dry periods. Understanding the interactions between surface and ground water during and after such events is crucial to estimate recharge rates, which are needed to design systems and/or management strategies to optimize the use of the limited water resources of those areas. However, challenges remain to directly measure parameters that control infiltration in arid areas, such as fluctuations in surface flow depth and velocity, soil unsaturated flow properties and moisture conditions, and the hydraulic gradient at the surface-subsurface interface. Moreover, the thickness of the vadose zone is typically large in arid environments and there can be a very long delay between the flood event that generates the infiltration and the recharge of the aquifer, which complicates recharge estimations. These challenges motivated us to apply an integrated surface and subsurface hydrologic model to simulate recharge mechanisms during and after an extreme flooding event that occurred in an alluvial valley in Northern Chile. The model was calibrated to reproduce general trends in groundwater levels and surface flow discharges, providing a physically plausible representation of the spatial and temporal fluctuations of infiltration and recharge. The calibrated model was then used to investigate the magnitude and spatio-temporal distribution of recharge and the response of the hydrologic system to different surface and subsurface parameters and initial conditions. The main contribution of this work is to apply an integrated surface and subsurface hydrologic model to investigate recharge mechanisms during and after an extreme flooding event in an arid watershed. We identify mechanisms that control recharge and discuss potential improvements to apply this type of models to similar areas elsewhere.

**This Chapter has been submitted to a technical journal for review and publication on 2018-04-23*

Introduction

In arid regions, evapotranspiration exceeds precipitation most of the time and surface water bodies are scarce and ephemeral. Groundwater therefore represents the primary supply for drinking water, natural ecosystems and economic activities such as irrigation. The quantification of groundwater recharge is thus essential to ensure the sustainable use of the water resource. In these regions, groundwater recharge is often limited to intense flood events that occur over short temporal intervals separated by long dry periods without any recharge (Gee and Hillel, 1988; Scanlon et al., 2006). These sporadic floods can be generated by single high intensity precipitation events that can sometimes represent more than half the annual rainfall. According to most climate change scenarios, extreme precipitation events will likely increase in magnitude in the future, with longer dry periods between events (Scanlon et al., 2006; Green et al., 2011; Taylor et al., 2013). These changes in precipitation patterns will have an impact on groundwater recharge in addition to generating more destructive floods, which will likely increase the pressure on groundwater resources (Taylor et al., 2013) .

Different approaches exist to estimate groundwater recharge in arid regions, including direct measurements, tracer-based methods, water balance methods, and hydrological modeling (Besbes et al., 1978; Gee and Hillel, 1988; Simmers et al., 1997; Simmers, 1998; Kinzelbach et al., 2002; De Vries and Simmers, 2002; Scanlon et al., 2002, 2006; Shanafield and Cook, 2014). However, because recharge occurs mostly over small spatial and temporal scales during extreme flooding events, it is challenging to install and operate monitoring equipment and apply direct estimation methods to observe these rare events. When flooding begins, surface water levels may rise within the span of minutes to a few hours. At the same time, infiltration increases along streambeds, over flood plains and complex terrains, which significantly affects flood wave propagation (Cheng et al., 2015). Infiltration rates change over time in response to changes in the water retention properties of shallow soil layers, with corresponding changes in the effective hydraulic conductivity and hydraulic head gradient at the surface–subsurface interface that determine different stream-aquifer connection states (Blasch et al., 2004, 2006; Shanafield and Cook, 2014). High initial infiltration rates associated to the high initial matric potential of dry top soils are particularly difficult to estimate or measure. When the initial ground water table is deep, significant delays between infiltration and groundwater recharge can also occur due to changes in storage through the unsaturated zone (Shanafield and Cook, 2014). Hence, it is necessary to consider flow in the unsaturated zone to determine changes in infiltration rates for different states of connection between surface and groundwater and calculate recharge to the groundwater table (Freeze, 1969; Cooley, 1971; Blasch et al., 2006; Brunner et al., 2009b; Shanafield and Cook, 2014).

Estimating recharge is further complicated by the difficulty in distinguishing between the impact of natural climate variability and that of human activities such as intensive groundwater extraction. Recent studies have concluded that aquifer recharge depends not only on the amount of available water, but also on the operation of groundwater extraction systems (Shentsis and Rosenthal, 2003; Taylor et al., 2013; Bartsch et al., 2014). These challenges point to the need for an improved understanding and characterization of the dynamics of watersheds in hyper-arid regions through innovative field-investigation and modeling techniques. Addressing the increasing pressure on groundwater resources, resulting from climate

change and land use change due to urbanization, will require innovative ideas based on a deep understanding of aquifers and their relation to surface streams. Taylor et al. (2013) summarizes this idea as: *"To sustain groundwater use under these conditions will require careful aquifer management that: (1) is informed by integrated models able to consider the range of interactions between ground water, climate and human activity and (2) exploits opportunities for enhanced groundwater recharge associated with less frequent but heavier rainfall events and changing meltwater regimes".*

Surface hydrology and groundwater models have historically been developed independently, which has created challenges in simulating variations in aquifer recharge and discharge. This challenge has motivated the development of Integrated Surface and Subsurface Hydrologic Models (ISSHM) (Maxwell et al., 2014; Paniconi and Putti, 2015; Fatichi et al., 2016), inspired by the seminal ideas put forward by Freeze and Harlan (1969) to conceptualize a fully-integrated hydrological response model. This type of model focuses on an integrated representation of the hydrological cycle, accounting for the interaction between surface and groundwater components (Winter, 1995; Sophocleous, 2002). The magnitude and distribution of exchange fluxes at different temporal and spatial scales are determined from a detailed representation of physical flow processes based on conservation of mass, energy and momentum. Watershed systems are described by parameters having direct physical meanings that can be estimated from previously compiled databases, field measurements, or description of materials and geometries. This integrated approach allows a more detailed characterization of the main physical processes and their interactions based on the synthesis of the available data at each scale. Integrated surface and subsurface hydrologic models are useful tools to assess groundwater recharge, evaluate and improve conceptual models, and overcome the difficulties of implementing observational techniques to address the lack of field data in arid regions. Morever, the application of a continuous iterative process makes it possible to update and recalibrate models with newly acquired data to refine the estimations (Bredehoeft, 2005; Ebel and Loague, 2006; Healy, 2010).

The main objective of this study is to apply an ISSHM to investigate and identify at the watershed scale, how physical processes and properties control groundwater recharge resulting from sporadic extreme surface flow events. We consider an alluvial aquifer located in the Valle de Azapa, which is the lower section of the San José River Basin, at the northern boundary of the Atacama Desert near the border between Chile, Perú and Bolivia. We use HydroGeoSphere (HGS) (Therrien et al., 2010; Brunner and Simmons, 2012; Aquanty Inc, 2013), which is an integrated surface and subsurface hydrologic model, to simulate flood infiltration and subsequent recharge to the Valle de Azapa aquifer. HGS simultaneously solves the two-dimensional diffusion wave approximation of the St-Venant equations to represent surface flow and the three-dimensional Richards' equation to represent variably-saturated groundwater flow (details of HGS, including the flow equations, are given in the Supplementary Material). We first present the conceptual and numerical model for the aquifer. We then use the model to simulate and examine the response of surface and groundwater during and after an extreme flooding event that occurred in 2001. The model is calibrated using observed groundwater levels and available surface flow discharge measurements. Our aim is not to generate a rigorously calibrated predictive model of the Valle de Azapa, but rather to develop a model that allow to study the recharge by considering surface–subsurface water interactions. In particular, we use the model to study the response of the system considering

different parameters, initial conditions and surface flow scenarios.

Numerical Model

Study Area

The San José River Basin covers an area of 3060 km^2 and marks the northern frontier of the Atacama Desert, which is considered to be the driest region in the world. Water in the basin mostly originates from convective summer rainstorms that occur from December to March, when moisture from the Amazon is carried westward to the upper part of the watershed located between 4000–5000 masl (Andean Plateau, *Altiplano*) (Houston, 2006b). At these altitudes, the average annual precipitation varies between 250 and 400 mm, and the intensity of single rainstorms can reach 15 mm/h. In the lower part of the basin, known as Valle de Azapa, precipitation is less than 5 mm/year and the San José River is an ephemeral stream that carries water only during summer floods.

The Valle the Azapa is oriented east-west and covers approximately 66.7 km^2. The valley extends eastwards over a distance of approximately 58 km from the Pacific Coast towards the Andes Mountains, where it reaches an elevation of 1215 masl (Fig 1). The main aquifer in the valley is unconfined and consists of fluvial and alluvial deposits that are mixtures of gravel, sand, silt and clays. The width of the aquifer varies between 500 m and 2,000 m and the permeable deposits varies from 0 m to 90 m depth. The aquifer extends along the valley axis from the coast to the city of Arica, over a distance of 38 km.

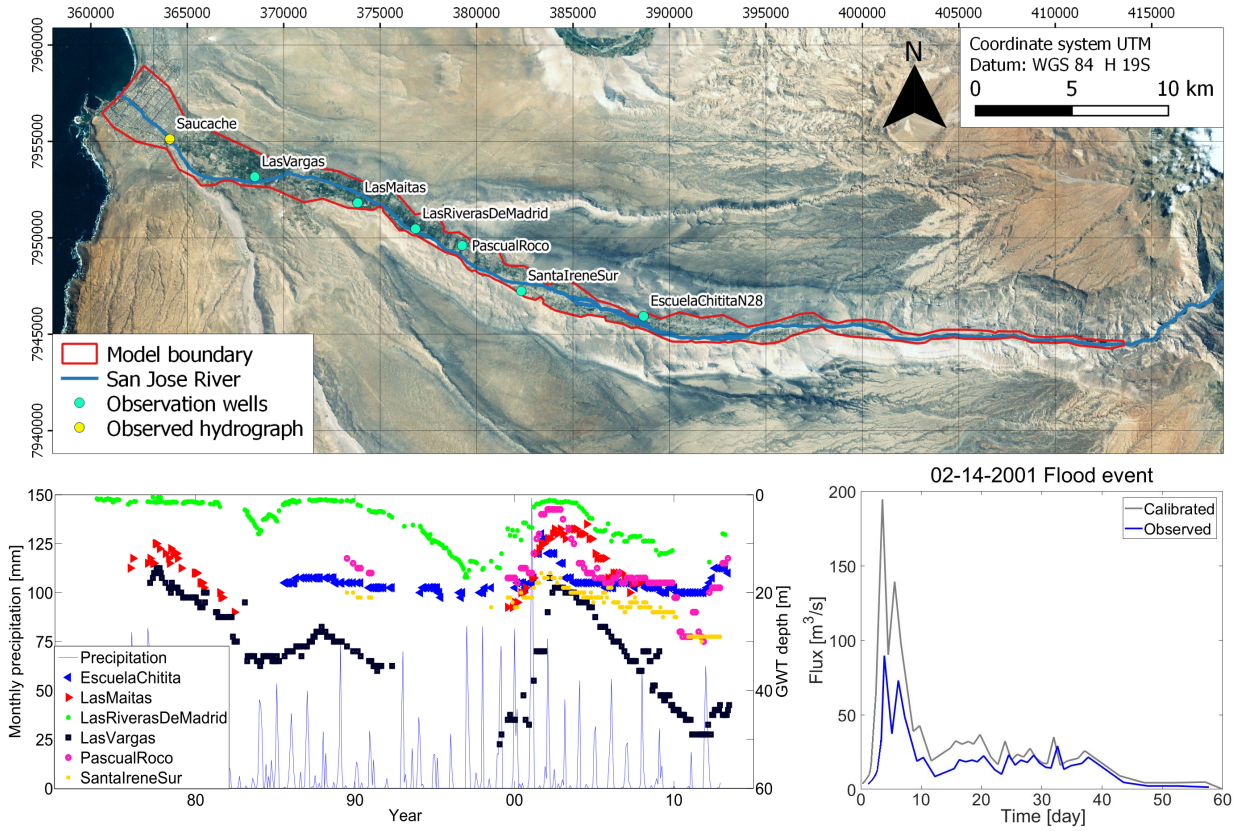

Figure 1: Location of monitoring wells used for model calibration along the San José River valley (top). Mean monthly rainfall and depth to water table observed at monitoring wells (bottom - left) and 2001 observed flow discharge measured at Saucache station and the calibrated flood hydrograph set as a transient surface nodal flux boundary condition at the center of the eastern model boundary (bottom - right).

Water infiltration in the streambed, river banks and floodplains are the main transmission losses in the river during floods, resulting in a progressive decrease in surface flow in the downstream direction. Some deposits of fine sediments transported by ephemeral creeks, located along the main axis of the valley, give rise to areas of lower permeability and transmissivity. In the upstream portion of the valley, over a distance of 14 km, the hydraulic conductivity of the upper sediments is low and transmission losses are negligible. However, the high permeability of the river bed in other sections of the San José River leads to high infiltration rates, resulting in recharge during floods (Taylor, 1949; Peña H., 1994; JICA, 1995; Arrau, 1997; AC, 2010; Jiménez Martínez, 2013; INH, 2014).

The Valle de Azapa has undergone active agricultural development in the last 30 years, with intensive use of surface and groundwater resources. Due to the fast expansion of agricultural activities, pressure on groundwater has increased. Because aquifer recharge is negligible between flooding events, extracted groundwater is mostly taken from the aquifer storage, which has caused significant and continuous declines of groundwater levels over periods of up to 10 years. The decline in groundwater levels has had a negative impact for about 67 % of all deep and dug wells (AC, 2010). For example, out of a total of 543 groundwater wells that exist in the valley, only 361 were still operating in 2008. The observed reduction of groundwa-

ter discharge to natural springs is another indication that the aquifer is overexploited during dry periods.

Model Setup

We developed a HGS integrated numerical model of the surface and subsurface system of the lower part of the San José River to represent the effect of a long-duration intense rainfall that occurred over the western Cordillera and the Altiplano (Houston, 2006a) and that started on Feb/14/2001 and extended until Mar/31/2001. The rainfall event had an estimated 60-year recurrence interval and caused one extreme flood event in the San José River that produced the hydrograph shown in Fig 1.

The simulation domain covers an area of 66.7 km^2 and corresponds to the alluvial deposits of the Valle de Azapa (Fig 1). The surface of the domain was discretized with 5,652 triangular finite elements, with an average element length of 200 m. The ground surface elevation was obtained from a 30 x 30 m ASTER Global Digital Elevation Model (GDEM) that was processed to remove artificial depressions and produce a continuous drainage network for the main stream towards the coast. The elevation of the bottom of the aquifer was defined from previews studies that considered the results of geophysical surveys based on transient electromagnetic (TEM) and gravimetric profiles (AC, 2010). The 3D subsurface mesh was generated by vertically superimposing the 2D triangular surface mesh from ground surface to the aquifer bottom to form the 3D triangular prismatic elements. A total of 24 layers of 3D elements was thus generated, with thicknesses varying from 0.5 m (top of the domain) to 3 m above the deepest groundwater table. The resulting vertical resolution was finer in areas of lower aquifer thickness and groundwater table depths. The final 3D mesh consists of 135,648 triangular prismatic elements and 80,800 nodes. To ensure that the mesh was sufficiently fine, simulation were also conducted with finer meshes. A comparison show that the mesh selected produced little difference in simulated water balance and groundwater levels response with respect to the finer meshes, while greatly reducing the simulation times.

Subsurface zones are defined in the model to represent the heterogeneous sediment distribution observed in the valley (Fig 2). Each zone is assumed homogeneous with parameter values that are based on the distinction between semi-consolidated and unconsolidated deposits and on the description included in subsurface borehole logs (JICA, 1995; AC, 2010). It is assumed that the aquifer is homogeneous along the vertical direction and the distribution of zones shown in Fig 2 therefore applies along the vertical direction, from the surface to the bottom of the model domain. A separate set of homogeneous zones is used to represent the surface flow domain, with surface properties such as roughness and storage coefficients based on the location of the main streams and rural and urban areas as shown in Fig 2.

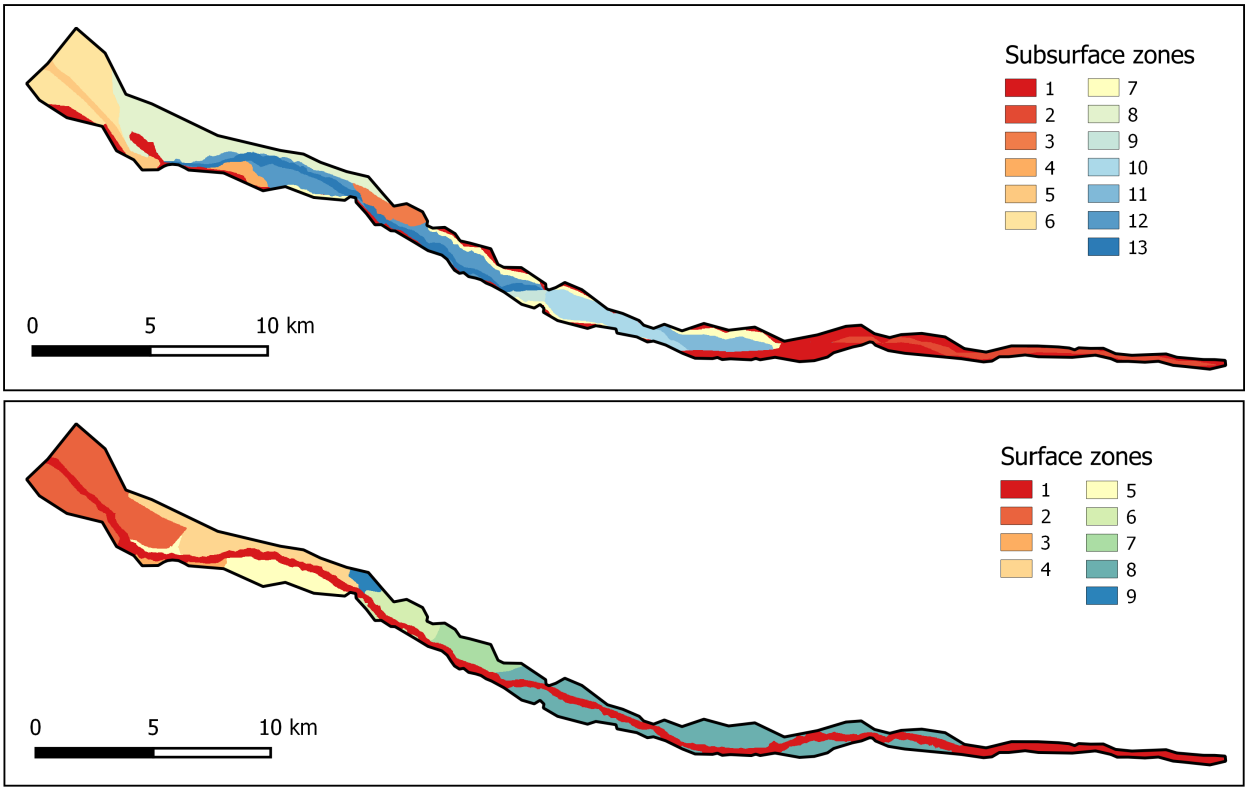

Figure 2: Spatial distribution of the homogeneous subsurface zones (top) and homogeneous surface zones (bottom).

The lateral and bottom boundaries represent the contact between the unconsolidated sediments and bedrock and they are assumed to be impermeable. Previous studies indicate that there is no connection between the aquifer and the sea (AC, 2010) and the corresponding western boundary is therefore assigned a critical depth boundary condition for the surface flow domain and a no-flow boundary for the subsurface domain. There was no flow observed in the lateral creeks during the flooding event and there is therefore no inflow of surface water specified for the downstream portion of the model.

To evaluate the impact of the flooding event on groundwater levels, we ran the model from the beginning of the flood, 14/Feb/2001, until 01/Jan/2003, when groundwater levels stabilized at the observation wells. During the simulated period, groundwater levels were measured at six wells located along the valley as shown in Fig 1. To represent the flooding water originating from the upstream portion of the River Basin, outside the simulation domain, an incoming transient nodal flux was assigned for surface water at the center of the eastern boundary. Because there is no observed hydrograph at that location, the incoming nodal flux value was iteratively modified until the model reproduced both the flood hydrograph measured at the downstream location of Saucache (AC, 2010), shown in Fig 1, and the observed groundwater levels.

The model was manually calibrated by visual comparison of the simulated groundwater levels and surface flow discharge with the observation wells data and the Saucache hydrograph (Fig 1). It was, however, only possible to partially calibrate the model parameters with the

limited available data. We used the van Genuchten model to characterize the unsaturated flow properties of the aquifer, which requires as input: the saturated hydraulic conductivity (K_s), specific storage (S_s), residual and saturated volumetric water content (θ_r and θ_s, respectively) and the van Genuchten parameters (α and β). Manning's roughness coefficients (n_x and n_y), rill storage height (h_r), obstruction storage height (h_o), and coupling length (l_e) are required to characterize surface domain properties (Panday and Huyakorn, 2004; Ebel et al., 2009) (for more details see the HGS model description in the Supplementary Material section). All these parameters can be initially estimated from previous field measurements. For example, values of hydraulic conductivities ranging from 0.01 to 100 m/d are reported in JICA (1995), an average value of infiltration rate over fluvial plains of 0.48 m/d was estimated by INH (2014), and saturated hydraulic conductivities ranging from 0.2 to 30 m/d were obtained from pumping tests. However, as mentioned above, there is limited data collected in the field that can be used to characterize the model parameters. Therefore, most of the physical parameters needed to describe the system and flood input hydrograph were initially assigned values taken from the literature and/or considering the hydrologic and hydrogeologic characteristics of the system.

For the simulation period, there was no data available to characterize recharge due to percolation from irrigation, losses from the water drinking network, and pumping/losses from wells and evapotranspiration and these fluxes were not considered in the model. Only the response of the aquifer system to the recharge induced by the flooding event is simulated and analyzed, which allows isolating the impact of the recharge due to flooding on groundwater levels.

At the beginning of the simulation, the flow system is not in dynamic equilibrium with respect to soil moisture and groundwater table depths, because of sporadic previous flood recharge events, transient pumping activity and changes in irrigation conditions. Because there is no available information to reproduce the initial equilibrium, the initial hydraulic head distribution was interpolated by ordinary kriging, using the observed groundwater levels at the beginning of the simulated period and taking into account the regional groundwater flow determined in previous studies (AC, 2010). A constant head value, which corresponds to a state of residual water saturation according to the van Genuchten model, was then assigned to the soil column from the ground surface to the interpolated phreatic levels. Thus, this approach considers an upper unsaturated zone that represents the volume available to store water that infiltrates during the event. This interpolated initial condition produces minimal changes in soil moisture and groundwater levels during the simulated period if no flood is simulated. The subsurface system can therefore be considered in an equilibrium state before the recharge process induced by the flooding event takes place. We analyzed the effect of different initial water table depths and antecedent soil moisture in the unsaturated zone as part of the model sensitivity evaluation discussed below.

Sensitivity Analysis

Using the calibrated model as the base scenario, we performed a detailed sensitivity analysis where the surface and subsurface flow properties, flood discharges, and initial conditions were varied to evaluate the response of the model and to better understand the interaction

between surface and subsurface flows in the system.

To test the flow properties, we simulated 13 additional scenarios to evaluate variations of subsurface parameters and 2 additional to evaluate variations of surface parameters. The parameters considered during this analysis are summarized in Table 1 and 2, respectively.

Table 1: Subsurface parameter scenarios for sensitivity analysis.

Zone	**Scenarios**												
	Hydraulic conductivitie [m/d]									**Porosity**			**Van Genutchen**
	K1	K2	K3	K4	K5	K6	K7	K8	K9	P1	P2	P3	V1 (α [m^{-1}] - β)
1	5.00E-04	5.00E-04	5.00E-04	5.00E-04	5.00E-04	5.00E-04	5.00E-04	5.00E-04	5.00E-04	**0.18**	**0.25**	**0.33**	5 - 1.72
2	3.00E-03	3.00E-03	3.00E-03	3.00E-03	3.00E-03	3.00E-03	3.00E-03	3.00E-03	3.00E-03	**0.18**	**0.25**	**0.33**	5 - 1.72
3	7.00E-02	7.00E-02	7.00E-02	7.00E-02	7.00E-02	7.00E-02	**3.50E-02**	**1.40E-01**	**4.50E-01**	**0.18**	**0.25**	**0.33**	5 - 1.72
4	7.00E-02	7.00E-02	7.00E-02	7.00E-02	7.00E-02	7.00E-02	**3.50E-02**	**1.40E-01**	**4.50E-01**	**0.18**	0.25	**0.33**	5 - 1.72
5	8.00E-02	8.00E-02	8.00E-02	8.00E-02	8.00E-02	8.00E-02	**4.00E-02**	**1.60E-01**	**4.50E-01**	**0.18**	**0.25**	**0.33**	5 - 1.72
6	8.00E-02	8.00E-02	8.00E-02	8.00E-02	8.00E-02	8.00E-02	**4.00E-02**	**1.60E-01**	**4.50E-01**	**0.18**	**0.25**	**0.33**	5 - 1.72
7	1.00E-01	1.00E-01	1.00E-01	1.00E-01	1.00E-01	1.00E-01	**5.00E-02**	**2.00E-01**	**4.50E-01**	**0.18**	**0.25**	**0.33**	5 - 1.72
8	1.20E-01	1.20E-01	1.20E-01	1.20E-01	1.20E-01	1.20E-01	**6.00E-02**	**2.40E-01**	**4.50E-01**	**0.18**	**0.25**	**0.33**	5 - 1.72
9	**3.20E-01**	**2.40E-01**	**2.00E-01**	**1.20E-01**	**8.0E-02**	**3.20E-02**	1.60E-01	1.60E-01	**4.50E-01**	**0.18**	**0.25**	**0.33**	5 - 1.72
10	**4.20E-01**	**3.15E-01**	**2.63E-01**	**1.56E-01**	**1.05E-01**	**4.20E-02**	2.10E-01	2.10E-01	**4.50E-01**	**0.18**	**0.25**	**0.33**	5 - 1.72
11	**4.70E-01**	**3.53E-01**	**2.94E-01**	**1.76E-01**	**1.18E-01**	**4.70E-02**	2.35E-01	2.35E-01	**4.50E-01**	**0.18**	**0.25**	**0.33**	**5 - 1.72**
12	**1.40E+00**	**1.05E+00**	**8.75E-01**	**5.25E-01**	**3.50E-01**	**1.40E-01**	7.00E-01	7.00E-01	**4.50E-01**	0.18	**0.25**	**0.33**	**5 - 1.72**
13	**1.60E+00**	**1.20E+00**	**1.00E+00**	**6.00E-01**	**4.00E-01**	**1.60E-01**	8.00E-01	8.00E-01	**4.50E-01**	0.18	**0.25**	**0.33**	**5 - 1.72**

Table 2: Surface parameter scenarios for sensitivity analysis.

Zone	**Scenarios**					
	N1			**N2**		
	$n_{x,y}$ [d/$m^{1/3}$]	h_r [m]	h_o [m]	$n_{x,y}$ [d/$m^{1/3}$]	h_r [m]	h_o [m]
1	**4.0E-07**	**0.009**	0.00	**3.0E-07**	**0.00001**	0.00
2	**4.0E-07**	**0.15**	**0.90**	**3.0E-07**	**0.07**	**0.35**
3	**4.0E-07**	**0.20**	**0.80**	**3.0E-07**	**0.08**	**0.30**
4	**3.2E-06**	**0.23**	**0.45**	**1.0E-06**	**0.05**	**0.10**
5	**3.2E-06**	**0.23**	**0.45**	**1.0E-06**	**0.05**	0.10
6	**3.5E-06**	**0.23**	**0.45**	**1.5E-06**	**0.05**	**0.10**
7	**3.2E-06**	**0.23**	**0.45**	**1.0E-06**	**0.05**	0.10
8	**3.2E-06**	**0.23**	**0.45**	**1.0E-06**	**0.05**	0.10
9	**3.5E-06**	**0.23**	**0.45**	2.5E-06	**0.05**	**0.10**

In other series of simulations, the initial water table depth was raised and lowered by successive increments of 2.5 m to obtain 9 different initial water table depths compared to the base scenario, with variations Δ_{WTfbe} = -7.5, -5, -2.5, +2.5, +5, +7.5, +10, +12, +15 m with respect to the base scenario, for which $\Delta_{WTfbe} = 0$ m. Negative values indicate a higher initial water table compared to the base scenario, while positive values indicate a lower initial water table. To better represent the downward water movement through the vadose zone, particularly for locations where the initial water table is deeper, we also used an alternative finer vertical discretization with 36 layers instead of 24 layers as described previously. We compare results for this finer discretization with those obtained with the coarser subsurface vertical discretization for the base scenario.

To evaluate the impact of the flood on simulated recharge, we also considered different values for the initial soil saturation through the unsaturated zone, for the case where the initial water table is 20 m below land surface for the whole domain. The base scenario is for an initial saturation everywhere equal to the residual saturation (0.1) above the water table. Three other scenarios were simulated, with a saturation that gradually increases from 0.1 at ground surface to 0.15, 0.2 and 0.25 at a depth of 2 m for scenario 1, 2 and 3, respectively, and remains constant from the depth of 2 m down to the water table. As a result, infiltration due to the high matric potential of dry top soils is similar for all simulated scenarios.

To evaluate the response of the system to consecutive flood events, six scenarios with different temporal distributions of the total calibrated flood volume for the base scenario were simulated. These simulations allow to reproduce the system response to management alternatives for surface water such as dams, dykes or infiltration barriers, informing about the impact on effective recharge rates and flooding. For each of these simulations, the total flood volume was distributed in 4 square pulses of 20 days each. The time lag between the beginning of each pulse was varied from simulation to simulation, with lag values of 20 days (i.e. no pause between each pulse), 50, 100, 200, 300 and 400 days. The simulation with the large lags between each pulse therefore takes longer.

Simulation Results

Calibration

The calibrated subsurface and surface flow parameters for the base scenario are summarized in Table 3 and Table 4, respectively. The metrics shown in Table 5 evaluate the difference between simulated and observed groundwater levels. Some of these indicators are not representative of the global model performance when errors or residuals ($O_\mathrm{i} - S_\mathrm{i}$) are biased and not normally distributed. In those cases, we analyzed the temporal evolution of the residuals for each observation well to evaluate the transient behavior of the model. A Lilliefors normality test (Lilliefors, 1967) of the residuals for surface discharge indicates failure to reject the null hypothesis at the 5 % significance level and the surface discharge residuals are considered unbiased and normally distributed. The global performance statistics values presented in Table 5 show that the model is suitable to simulate surface flow. For subsurface comparison, the normality test for residuals indicate rejection of the null hypothesis at the 5 % significance level, so residuals are biased and not normally distributed and the statistics presented previously remove some information about how the errors are distributed.

Table 3: Calibrated subsurface parameters. Saturated hydraulic conductivity (K_s), specific storage (S_s), van Genuchten parameters (α and β) and residual and saturated volumetric water content (θ_r and θ_s, respectively).

Zone	**K [m/d]**	S_s $[m^{-1}]$	α $[m^{-1}]$	β	θ_s	θ_r
1	5.0E-04	1E-05	5.0	1.72	0.20	0.020
2	3.0E-03	1E-05	5.0	1.72	0.20	0.020
3	7.0E-02	1E-05	5.0	1.72	0.22	0.022
4	7.0E-02	1E-05	5.0	1.72	0.25	0.025
5	8.0E-02	1E-05	5.0	1.72	0.24	0.024
6	8.0E-02	1E-05	5.0	1.72	0.27	0.027
7	1.0E-01	1E-05	5.0	1.72	0.20	0.020
8	1.2E-01	1E-05	5.0	1.72	0.23	0.023
9	1.6E-01	1E-05	5.0	1.72	0.27	0.027
10	2.1E-01	1E-05	5.0	1.72	0.27	0.027
11	2.3E-01	1E-05	12.2	2.28	0.27	0.027
12	7.0E-01	1E-05	12.2	2.28	0.18	0.018
13	8.0E-01	1E-05	12.2	2.28	0.18	0.018

Table 4: Calibrated surface parameters. Manning's roughness coefficients (n_x and n_y), rill storage height (h_r), obstruction storage height (h_o).

Zone	$n_{x,y}$ $[\mathrm{d}/m^{1/3}]$	h_r $[m]$	h_o $[m]$
1	3.5E-07	0.0001	0.00
2	3.5E-07	0.09	0.70
3	3.5E-07	0.17	0.60
4	2.0E-06	0.14	0.32
5	2.0E-06	0.13	0.32
6	2.5E-06	0.16	0.32
7	2.0E-06	0.11	0.32
8	2.0E-06	0.11	0.22
9	2.5E-06	0.17	0.32

Table 5: Global model performance statistics for the calibrated base scenario. MAE: Mean absolute error, ME: Mean error, $RMSE$: Root mean square error, $NRMSE$: Normalized root mean square error, NSE: Nash–Sutcliffe coefficient for surface flow discharge. ΔO is the range of observed groundwater levels, O_{i} and S_{i} are observed and simulated values, $\overline{O}$ is the mean observed value and N is the number of observations.

Statistic	**Subsurface**	**Surface**
$MAE = \sum_{\mathrm{i}=1}^{N} \frac{\lvert O_{\mathrm{i}} - S_{\mathrm{i}} \rvert}{N}$	2.5 m	-
$ME = \sum_{\mathrm{i}=1}^{N} \frac{O_{\mathrm{i}} - S_{\mathrm{i}}}{N}$	-1.5 m	-
$RMSE = \sqrt{\sum_{\mathrm{i}=1}^{N} \frac{(O_{\mathrm{i}} - S_{\mathrm{i}})^2}{N}}$	3.7 m	1.4 m^3/s
$NRMSE = \frac{RMSE}{\Delta O}$	8.4 %	-
$NSE = 1 - \left[\frac{\sum_{\mathrm{i}=1}^{N} (O_{\mathrm{i}} - S_{\mathrm{i}})^2}{\sum_{\mathrm{i}=1}^{N} (O_{\mathrm{i}} - \overline{O})^2} \right]$	-	0.93

The observed and simulated depth to water table at the observation wells for the calibrated model are shown in Fig 3. The simulated trends in water table depth at the wells could not be improved without affecting the performance of the model at other locations or with respect to others variables. However, the calibrated flood hydrograph (Fig 1) and parameters set allows simulating an infiltration recharge process that reasonably reproduce the behavior of the observed water table rise at most observation points. The good agreement between simulated and observed surface flow discharge and groundwater levels indicate that, even with limited data for the model conceptualization, it is possible to obtain reasonable results that explain qualitatively and quantitatively the response of the aquifer system to the recharge induced by the flooding event.

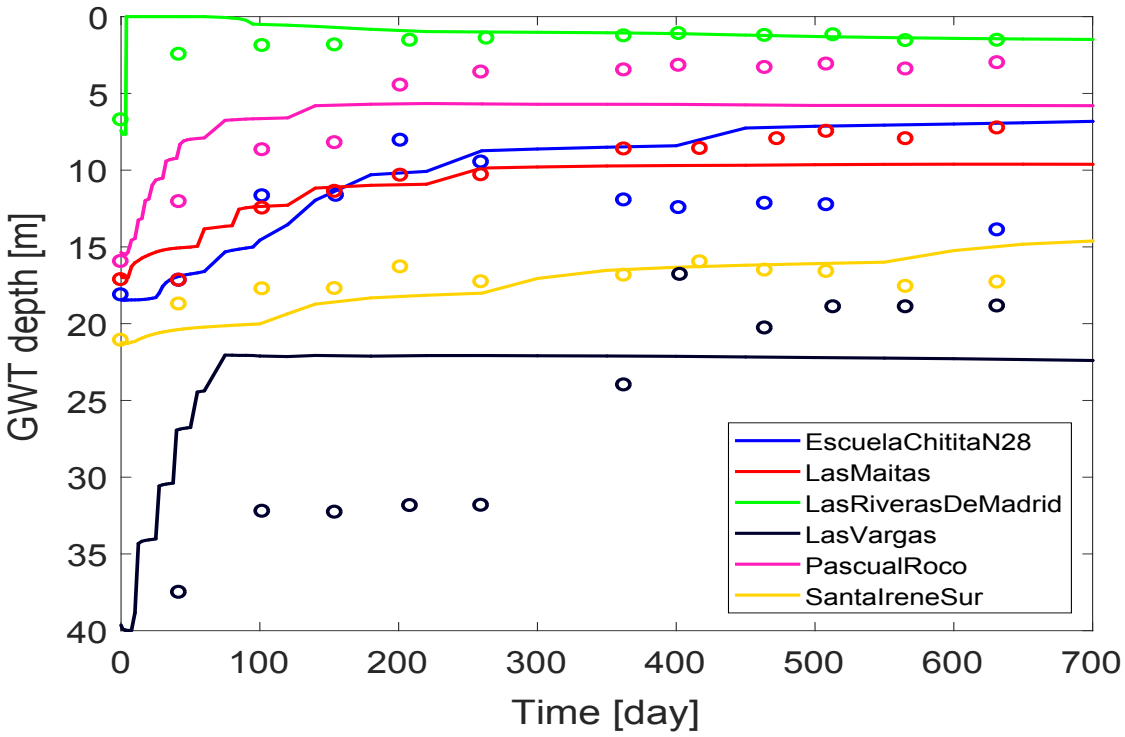

Figure 3: Observed (circles) and simulated (solid lines) groundwater levels at selected monitoring wells.

Base Scenario

The simulated infiltration, shown in Fig 4, shows that infiltration mostly occurs over a reduced area, located over the main river channel and active surface flow paths. The areas with lower infiltration rates correspond to those flooded only for short periods during the flood peaks. In addition to the spatial distribution of recharge shown in Fig 4, temporal variations of total infiltration and water table depth at 3, 12 and 29 km from the coast along the river axis are shown in Fig 5. The observed and simulated surface flow discharge at Saucache and the temporal variation in the global simulated infiltration rate are further shown in Fig 6 (left panel), along with the temporal evolution of the surface water depth, location of the saturated wetting front presented as the inverted water table depth (IGWT), and infiltration rate along the river axis. The range of infiltration rates presented is limited for an adequate visualization of the lower rates but peak values of up to 25 m/d were simulated.

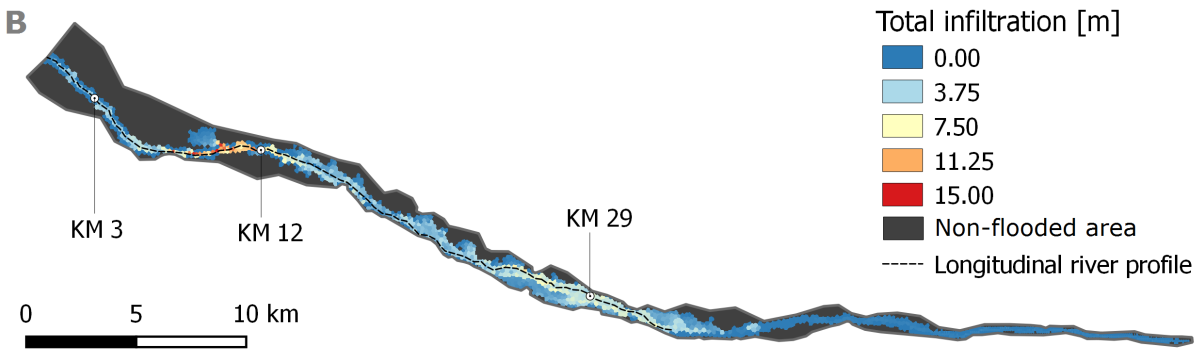

Figure 4: Total infiltration and total flooded area delimitation. Colors represent the magnitude of the cumulative flood infiltration at flooded areas.

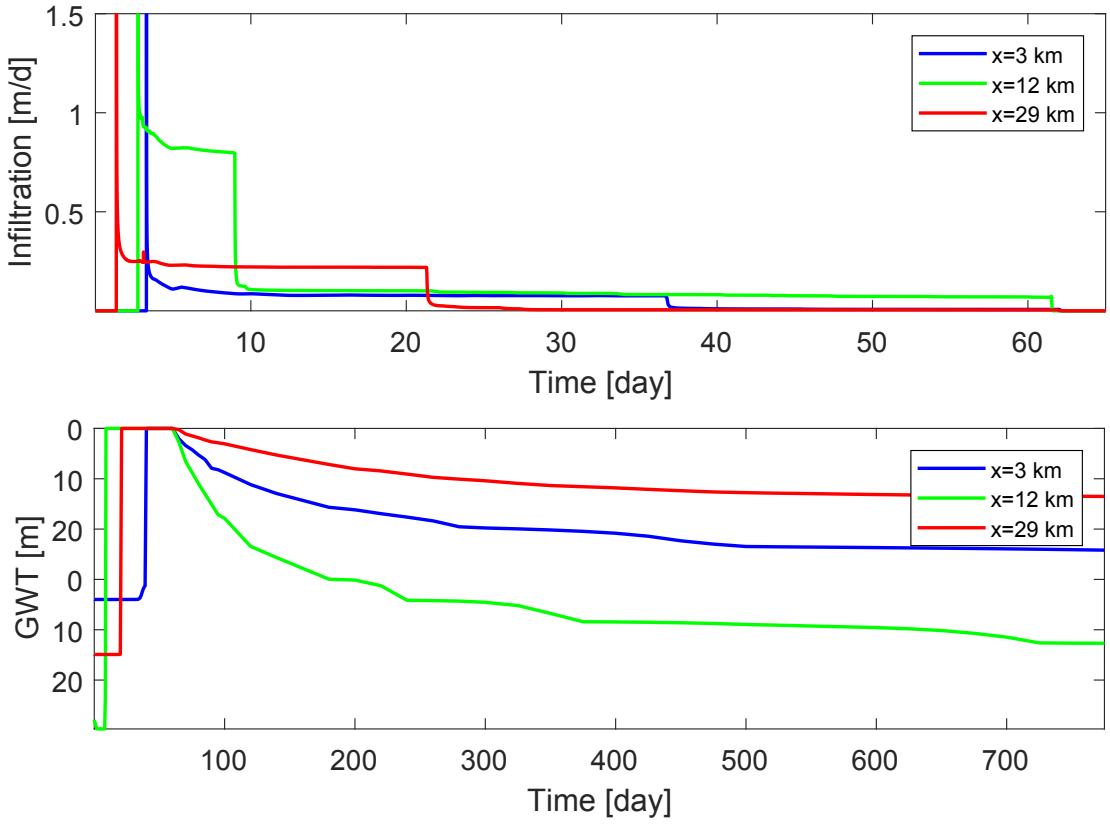

Figure 5: Temporal evolution of simulated infiltration rates and groundwater table depth (GWT) for the entire simulation at distances of 3, 12 and 29 km from the coast along the river axis.

The model results shown in Fig. 5 and Fig. 6 define an infiltration process similar to that described by Blasch et al. (2006), with transient and steady state infiltration rates during the

flood event. Initially, the flood wave starts to feed the stream and the surface water depth increases rapidly, which in combination with the dry condition of the shallow soil layers produce larger hydraulic gradients and high infiltration rates. This transient infiltration behavior lasts between 3 and 24 hours at a single location and infiltration reaches its peak value in less than one hour (see Fig. 5). The total infiltration in the system stops increasing when the flood wave reaches the sea and flooded top soils have been moistened. When water saturates the top soil layers, a saturated front (IGWT) controlled by gravity advances downward following preferential surface flow paths. A quasi–steady state period of lower infiltration rates limited by the hydraulic conductivity of the soils (K_{sat}) is observed. A transition from disconnected to connected state between surface and groundwater systems takes place along the active river channel. When the saturated front reaches the water table, the stream and aquifer are connected, pressure is transmitted to the regional aquifer, infiltration rates decrease considerably and lateral flow to the the waterwater table and groundwater mounding begins. At that time, represented by gray values in Fig 6, infiltration is limited by the aquifer transmissivity and its ability to transport and redistribute the infiltrated water out of the flooded area. Surface and groundwater systems connect at different times depending mainly on the soil hydraulic properties and the initial groundwater table depth. Connection occurs earlier in the central zone (between 10 to 25 km from the coast along the longitudinal river profile), where the soil porosity is lower and the saturated hydraulic conductivity is greater. The connection occurs earlier for shallower groundwater levels. Total infiltration decreases with time as surface and groundwater systems connect.

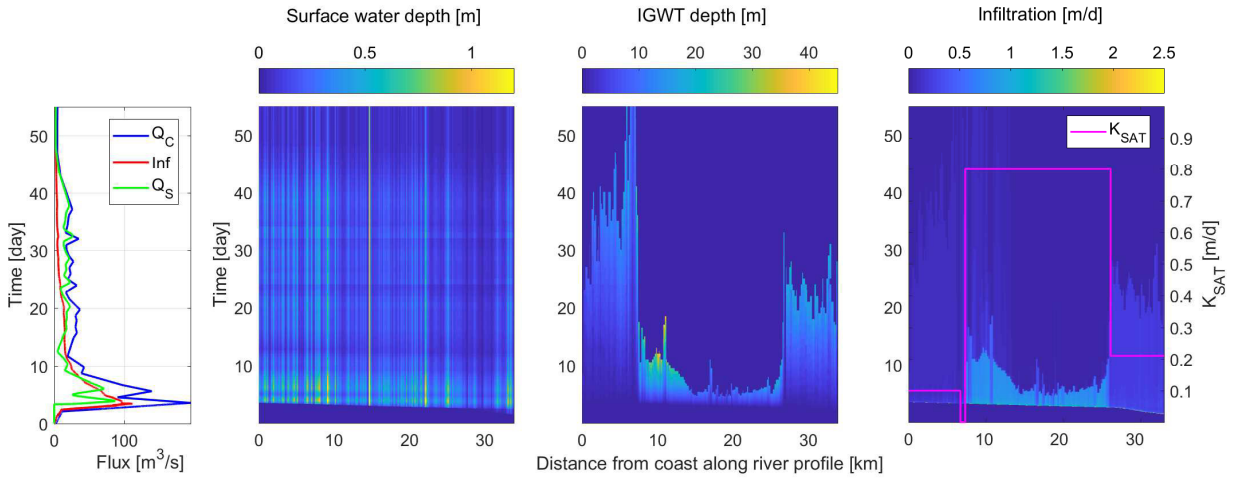

Figure 6: Calibrated flood hydrograph (Q_C), total infiltration rate (inf) and simulated surface flow discharge (Q_s) (left); temporal evolution of surface water depth, depth of the inverted water table (IGWT), infiltration rate, and saturated hydraulic conductivity along the river axis (from left to right, respectively).

Fig 7 shows the temporal variation of subsurface saturation for a vertical cross-section along the river axis. The initial water table depth and the IGWT and GWT during flood event can be observed before the stream–aquifer connection. After the flood event, groundwater levels gradually decrease under the active flow paths. The surface and subsurface are hydraulically connected along the main channel during the flood and connectivity is maintained longer between 18 and 21 km from the coast, approximately, along the river axis. In this area, groundwater levels are shallow and groundwater feeds springs (Taylor, 1949; AC, 2010). Two years after the flood, groundwater is still feeding these surface springs. Surface-subsurface water interactions can be better visualized in Fig S1 in the Supplementary Material, which shows the water table depth along the river axis for the entire simulation.

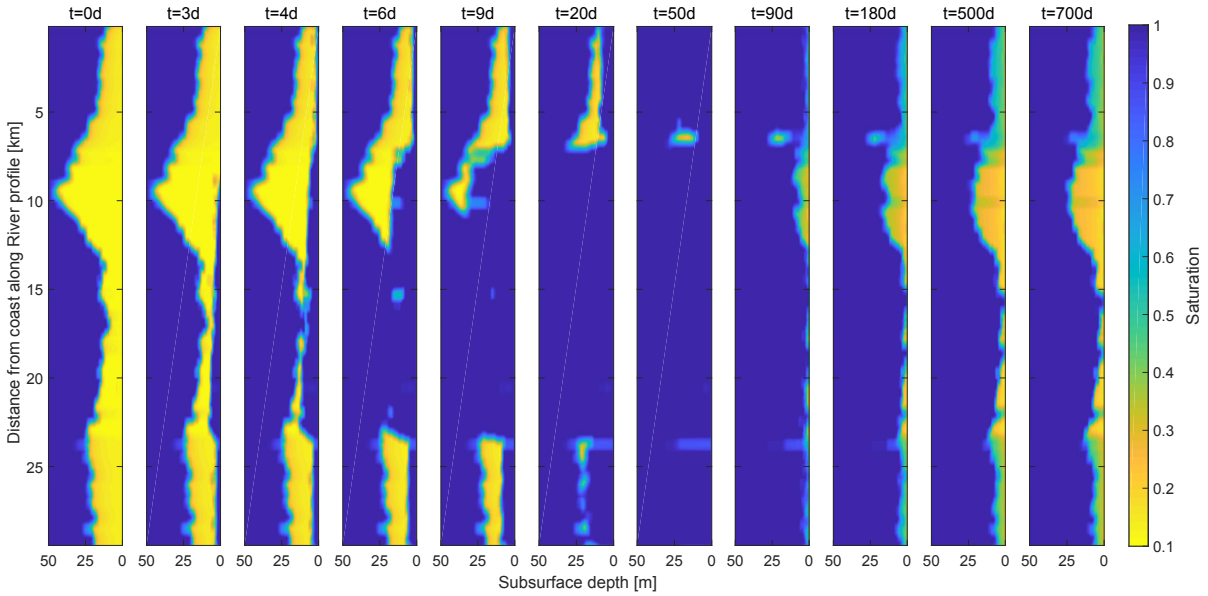

Figure 7: Subsurface saturation at different simulation times for a vertical cross-section located under the river axis. A physical distortion exists because elevations are projected horizontally in a 2D rectangular plane. Note that the vertical axis representing the distance along the river is in kilometers, while the horizontal axis that shows depth under the river bed is in meters.

The total simulated flood volume for the calibrated model is 1.42E+08 m^3. At the end of the simulated period, 41.2 % of this total flood volume had infiltrated and reached the saturated zone, representing effective groundwater recharge. A volume equal to 5.4 % of the total still remained as moisture through the unsaturated zone. That residual moisture is located either above the water table under the active surface flow paths, where most of infiltration took place, or in areas of non–active flow and shorter flooding duration, where water diffuses through the unsaturated zone and takes longer to contribute to groundwater recharge.

In Fig 8, a map shows the difference between final and initial groundwater levels over the whole domain after groundwater redistribution (t=700d), when groundwater levels stabilize

and changes in unsaturated and saturated storage are minimal. The map shows that recharge is localized under infiltration areas covering the main aquifer. The spatial variations in the magnitude of recharge are due to flood conditions, initial water table depth and subsurface properties, which determine the stream–aquifer connection time and aquifer redistribution capacity.

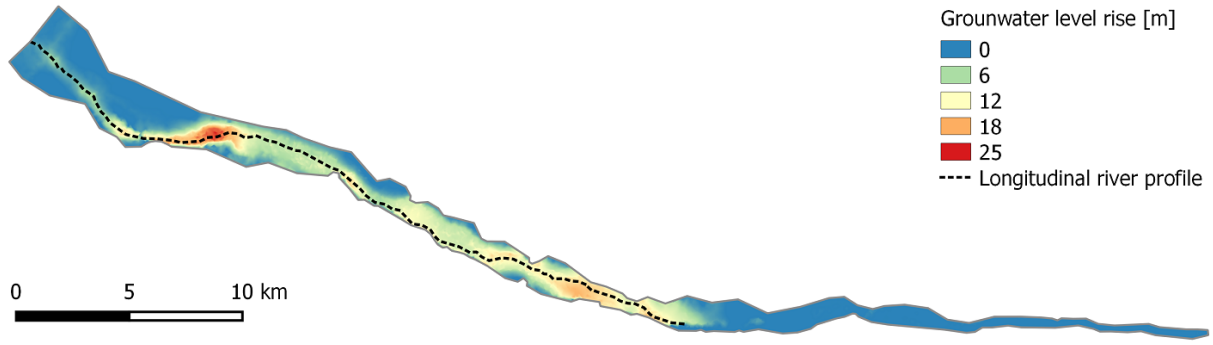

Figure 8: Difference between the final and initial groundwater levels, corresponding to the total simulated groundwater level rise.

Sensitivity Analysis

We compared the calibrated base scenario and the 15 scenarios summarized in Tables 1 and 2 to determine the parameters that most influence simulated groundwater levels and surface flow discharge. Fig 9 and Fig 10 show the overall effect of simulated parameter scenarios on groundwater levels and surface flow discharge versus time at each observation point. Positive residuals correspond to values lower than those simulated by the base scenario, while negative ones indicate values that are higher than simulated in the base scenario.

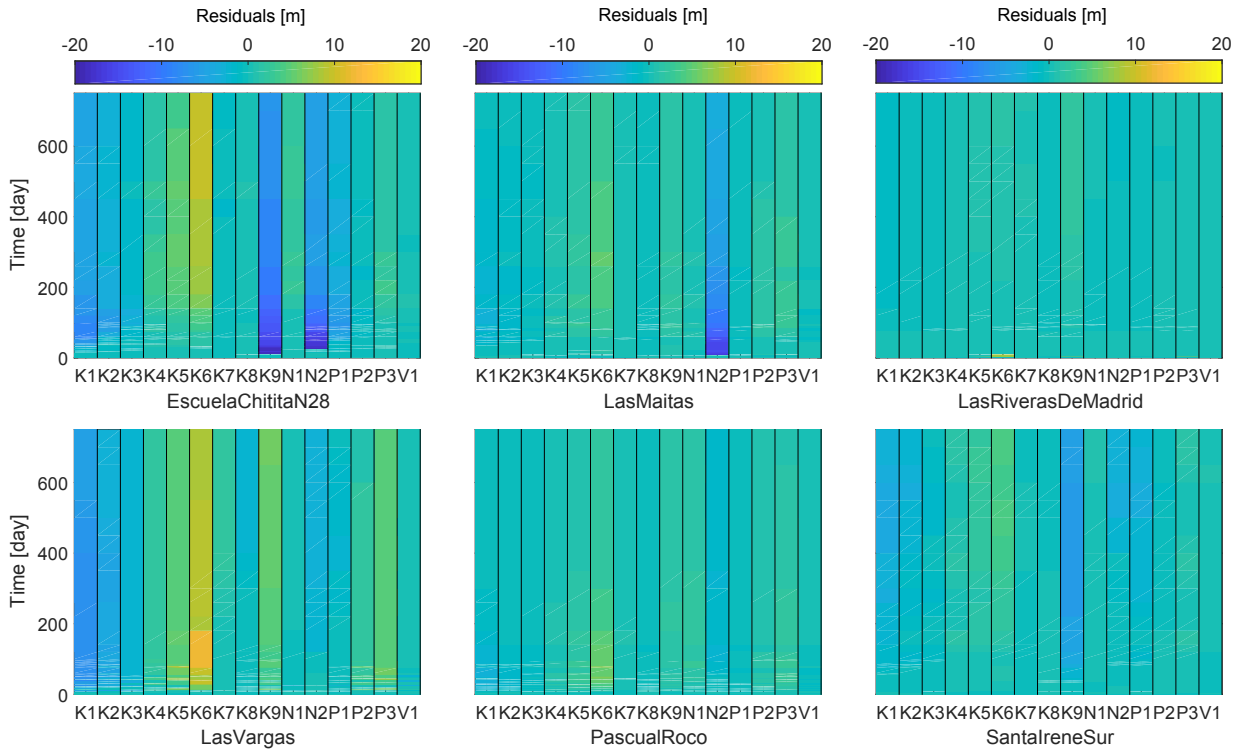

Figure 9: Differences (residuals) between groundwater levels simulated at each well for the base scenario and levels simulated for the other scenarios.

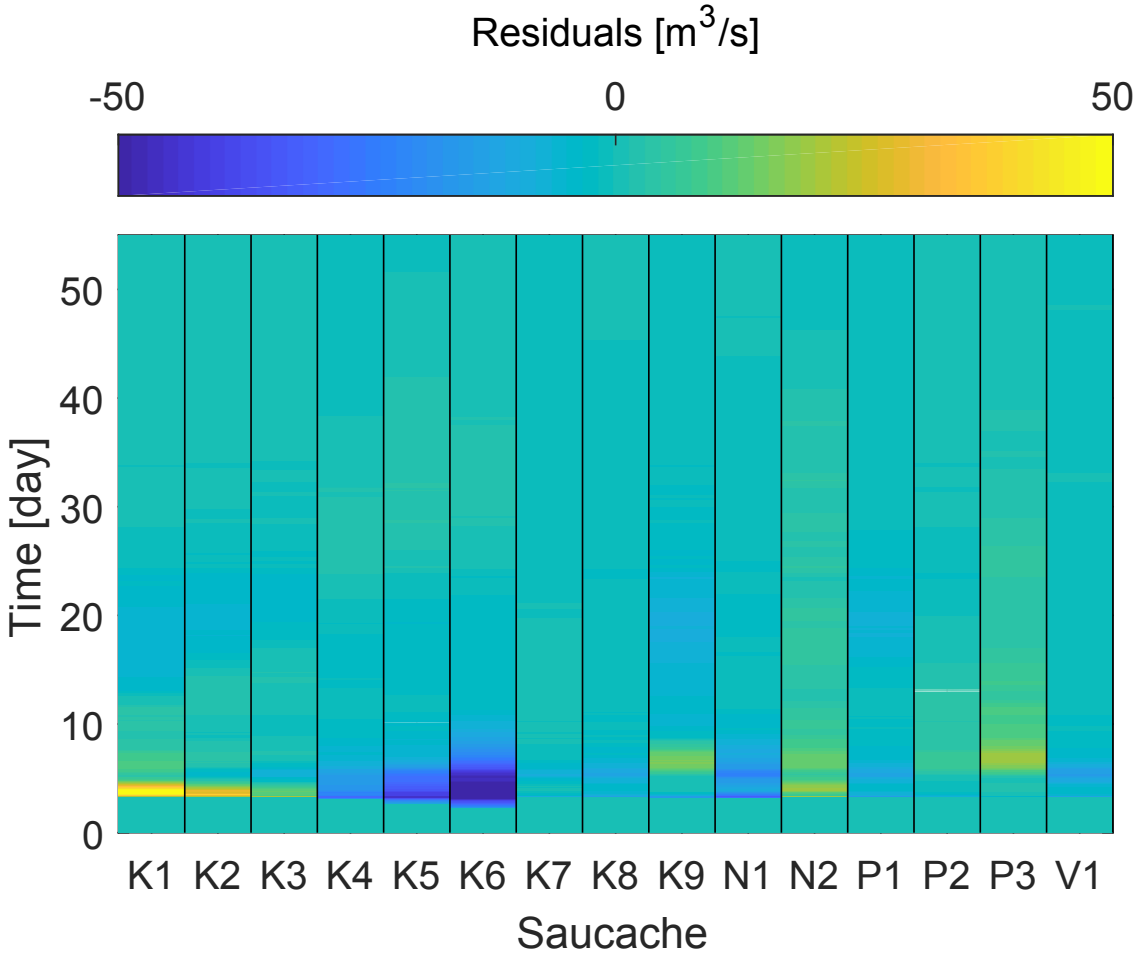

Figure 10: Differences (residuals) between the simulated surface flow discharge at the Saucache gauging station for the base scenario and discharge simulated for the other scenarios.

The simulated hydraulic head at observations wells Escuela Chitita N^{o}28 and Las Vargas shows a greater sensitivity to changes in the flow properties than at other wells. These two wells are in areas that are especially sensitive to a reduction of surface roughness and storage properties and changes of the main aquifer hydraulic conductivity. Variations in the properties of both surface and subsurface domains modify the magnitude and propagation time of the flood wave downstream. During the flood peak, when surface and groundwater systems are disconnected and most of the infiltration occurs, the effect of the different parameter scenarios on the hydrograph shape is more relevant.

The total infiltration and effective recharge as a percentage of the total flood volume are shown in Fig 11 for all scenarios.The calculated residuals and total infiltration show that the model is more sensitive to the following four scenarios : the two extreme hydraulic conductivity scenarios K1 and K6, the higher porosity scenario P3 and scenario N2 that considers a reduction in surface flow resistance and storage properties. To further investigate the system behavior and model sensitivity, the magnitude of the cumulative flood infiltration at the inundation areas for those four scenarios (K1, K6, P3 and N2) is shown in Fig 12. The infil-

tration values presented are limited to 15 m for an adequate visualization of lower infiltration and for comparison with the base scenario (Fig 4), but the K1 and P3 scenarios produce higher values in the areas of greater infiltration. Fig 13 further shows the temporal total infiltration in time and the dynamics of surface–subsurface interaction along the longitudinal river profile. Figures 12 and 13 therefore provide a more detailed representation of the infiltration processes and variables state for the different scenarios. Changes in parameters produce differences in transmission losses along the aquifer, surface flow depths, and extent of inundated areas. This results in a reduction/accretion of surface flow and delays/advances in flood wave propagation, which added to the extremely rapid rise to peak flow, translates into the differences of surface flow discharge respect to the base scenario (B) (Fig 10). Infiltration increases for the higher hydraulic conductivity scenario, while the extent of the flooded areas decreases and the flood takes longer to reach the sea. As hydraulic conductivity is reduced, infiltration and effective recharge decrease and a large proportion of the infiltrated water remain stored as moisture throughout the vadose zone at the final simulation time. More detailed transient infiltration rates and water table depths at point locations are also shown in Fig S2 of the supplementary material.

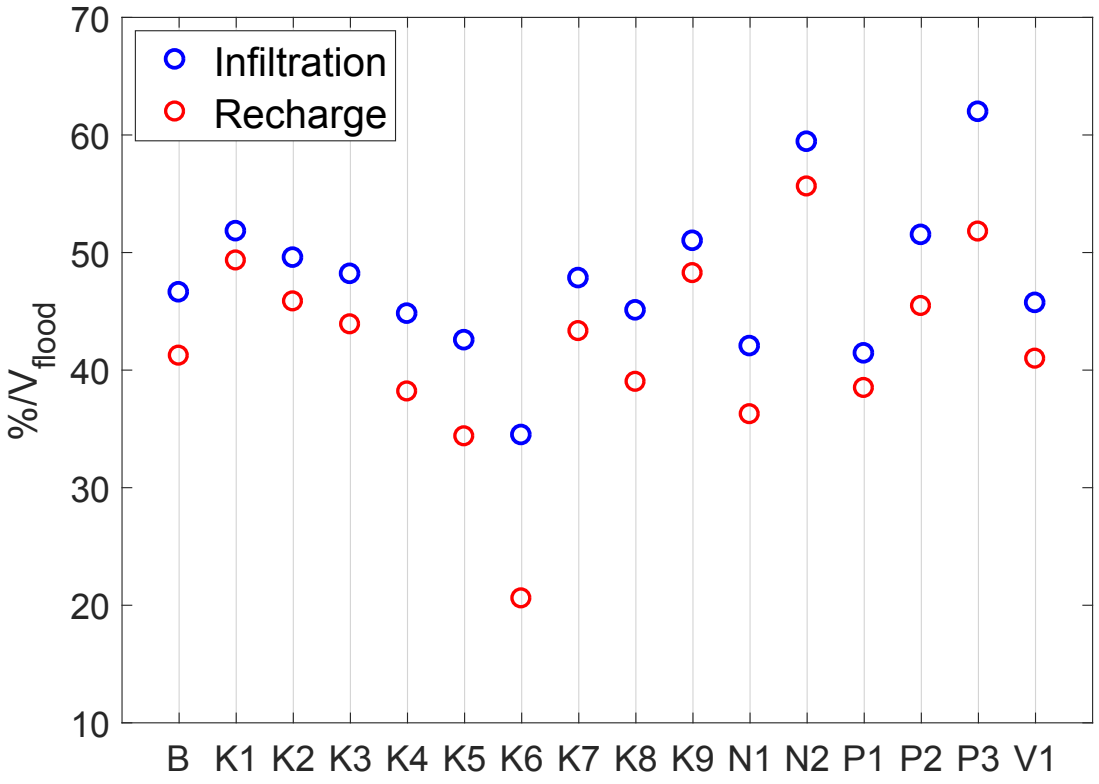

Figure 11: Volume of infiltrated water and effective recharge for the final simulated time expressed as a percentage of the total flood volume for each simulated scenario.

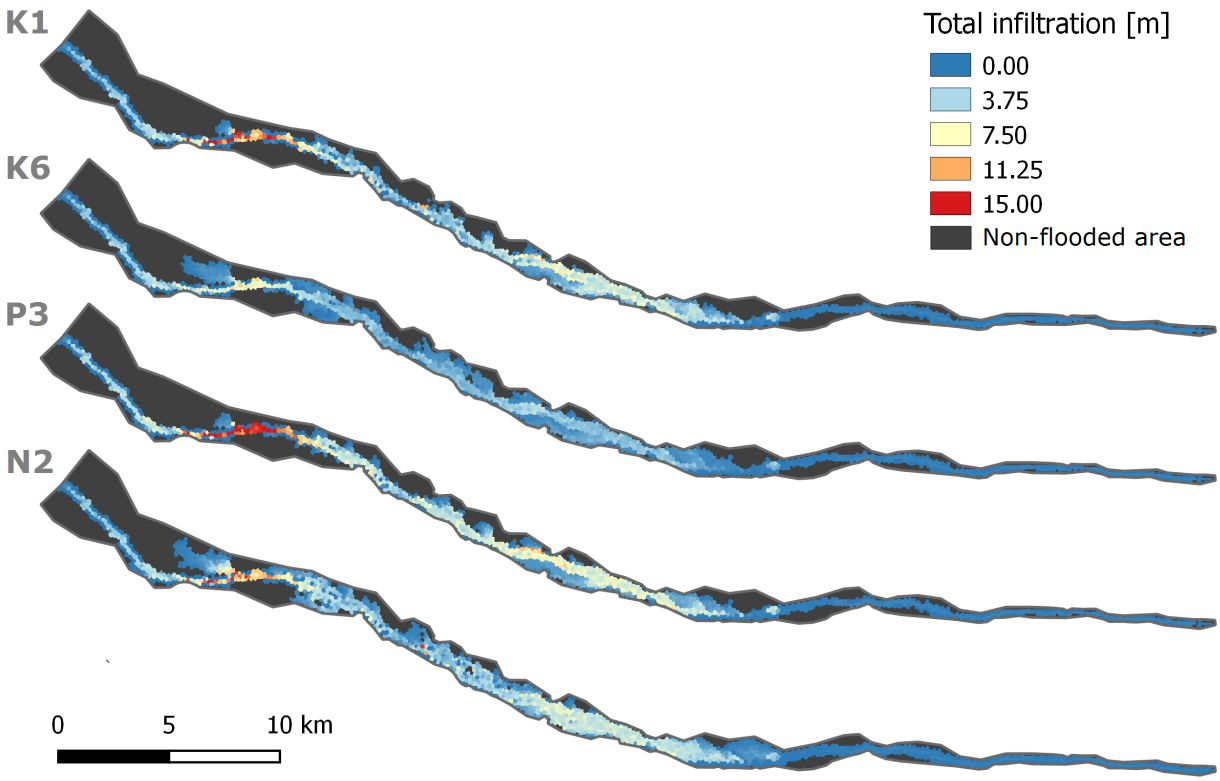

Figure 12: Spatial distribution of total infiltration and flooded areas for the scenarios with greatest variations (K1, K6, P3 and N2).

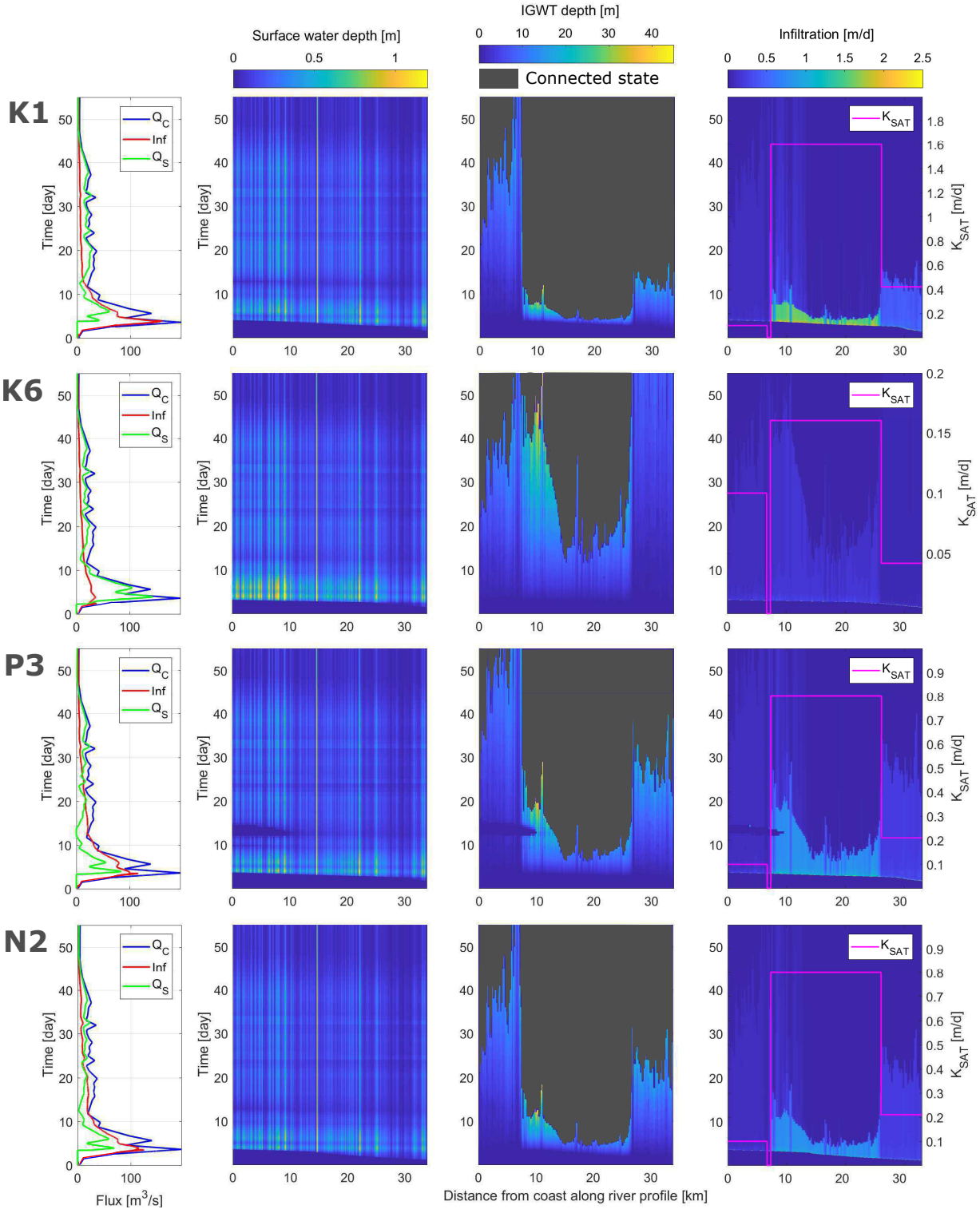

Figure 13: Calibrated flood hydrograph (Q_C), total infiltration rate (inf) and simulated surface flow discharge (Q_s) (left panels); and temporal evolution of surface water depth, depth of the inverted water table (IGWT), infiltration rate, and saturated hydraulic conductivity along the river axis (from left to right, respectively) for scenarios K1, K6, P3 and N2 (from top to bottom).

The soil parameters for the 8 downstream kilometers are the same for the B, K1 and K6 scenarios and infiltration rates and the time of stream-aquifer connection in this area are therefore similar for these scenarios, because the flood stage in the main active channel is high enough to satisfy the infiltration capacity for the same hydraulic conductivity conditions, despite the differences in flood stage due to different soils properties and infiltration upstream. This result is also observed along the entire longitudinal river profile for the N2 scenario, which results in a reduction of river flow depth with respect to the base scenario, but infiltration rates and the connection of surface and groundwater systems are similar in magnitude and timing. Total recharge is however greater because flooded areas and preferential and active flow paths increase. For scenario N1, infiltration and total recharge only decrease by 1.5 % because flooded areas slightly decrease. Although there are higher surface flow depths in the main channel respect to the base scenario, it is not reflected in a greater infiltration because the similar properties of soils and infiltration capacity.

Higher porosities (scenario P3) increases the aquifer storage capacity, which maintains a disconnected surface–groundwater state and reduces the associated infiltration rates over longer periods, in turn reducing flooding areas and surface flow discharge earlier than for the base scenario. The infiltrated water that contributes to effective recharge and the water stored as moisture through the unsaturated zone increase with respect to the base scenario. Twelve days after the flood began, there is no surface flow available to infiltrate along the last 10 km of the river and the saturated front diffuses out in the unsaturated zone, then saturates again when surface flow increases. Although, the P3 scenario produces greater total infiltration than the N2 scenario, the effective recharge is less than in the latter case, because it accumulates in greater proportion through the vadose zone as consequence of higher porosity.

The different van Genutchen soil parameter scenario (V1), on the other hand, uses the same saturated hydraulic conductivity as the base scenario considering a sandy loam pressure–saturation curve for the most permeable zone instead of a sand texture relation, which traduces in a different initial saturation condition above the groundwater table with more water stored in an unsaturated state due to a higher capillarity tension. This scenario has little influence in the model output compared to the other scenarios because infiltration under unsaturated conditions occurs for a short time at the beginning of the flood, soils quickly saturate, causing the wetting front movement through the vadose zone to be controlled by gravity, while the saturated hydraulic conductivity is the same as that for the base scenario. Since at the end of the simulation a condition near equilibrium has been reached for both scenarios, the infiltrated water that contributes to effective recharge is similar.

The simulation results for the scenario with a variable initial water table elevation show that the flood contribution to recharge is controlled by the initial depth to the groundwater table (Fig 14). As the initial water table is lowered, the disconnected state between the surface and groundwater system lasts longer and higher infiltration rates are maintained for a longer period. Fig 14 (left) shows the time when the inverted water table and actual water table connect along the river axis for the base scenario and the extreme cases ($\Delta_{WTfb\mathrm{e}} = +7{,}5, 0, -15\,m$). The infiltrated volume, expressed as a percentage of total flood volume, has a positive quasi-linear behavior as a function of the depth of the initial groundwater table (Fig 14, right). A small reduction of infiltrated water with depth is due to the fact that, for lower levels, the volume of the flood is not enough to fill the last section downstream. The

same quasi-linear behavior is observed for effective recharge, but with a larger rate reduction that increases for the lower initial water table because water mound takes more time to dissipates in a thicker vadose zone. At the end of the simulated time, a greater proportion of the infiltrated water still remains as moisture in the vadose zone for the lower initial water tables. Differences in total recharge of up to 3 % exist when a finer vertical discretization is considered respect to using the discretization prepared for the base scenario, which can be considered minor in comparison to differences produced by changes in other parameters.

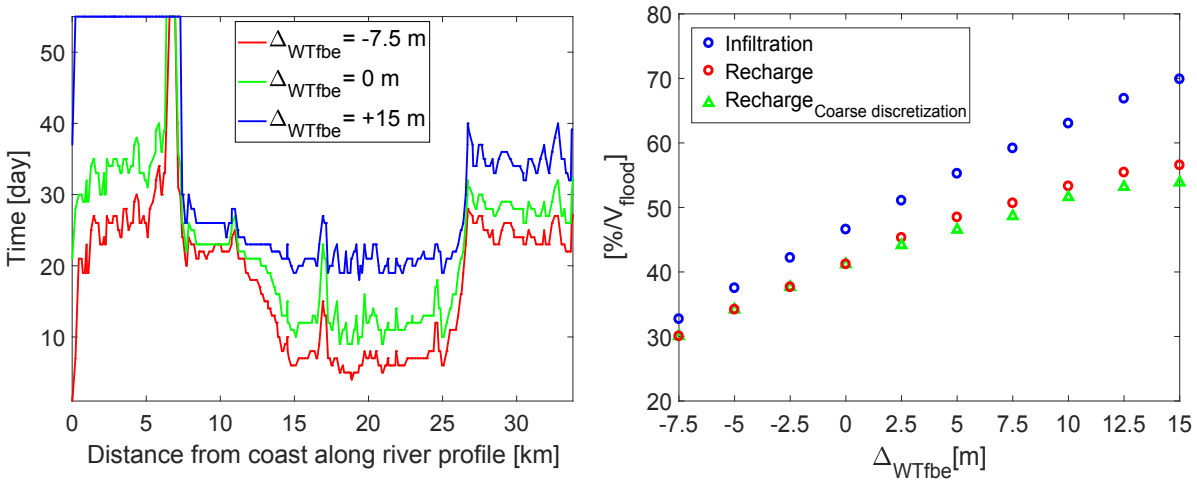

Figure 14: Time of connection between surface and groundwater systems along the river axis for scenarios with maximum and minimum initial water table depth and for the base scenario [left]. Total infiltration and effective recharge as percentage of the total flood for different initial water table depth using the 24 layers vertical discretization for the based scenario (red circles) and a finer discretization (36 layers) (green triangles) [right].

For higher initial saturation, the volume available to store water through the vadose zone is reduced and the saturated hydraulic conductivity value is reached sooner through the soil profile. As a result, the inverted groundwater table drops faster through the unsaturated zone and surface and groundwater systems connection occurs earlier, along with a reduction in infiltration rates and total recharge. Groundwater levels also rise sooner at observation points. There is a difference of 6.5 % in total infiltration, as a percentage of the total flood volume, between the driest and the wettest initial soil moisture scenarios (saturation profiles of 0.1 and 0.25, respectively). Due to the equal top soil profile considered for the initial moisture simulations (see methodology section), the high rates of initial infiltration due to the high matric potential of dry top soils is similar for all simulated scenarios. Differences in total recharge would therefore be greater if higher saturation values were considered for the top soil layers. Less infiltration for a particular flood event is expected if, for example, irrigation activities and previous flood events, which can even produce higher initial saturation conditions than those tested, are taken into account to establish the initial pressure head–saturation condition. For example, saturation levels ranging from 0.2 to 0.5 under the river bed still prevail two years after the 2001 flood event (see Fig 9).

Fig 15 shows results for the scenarios that assume that the total flood volume is distributed as four pulses of 20 days separated by different lags. The surface–groundwater system remains disconnected longer with higher infiltration rates when the time lag between pulses is greater. Fig 16 shows subsurface saturation along the river axis prior to releasing the second pulse for the different pulse distributions considered (δ_p). When the flood volume is distributed over several pulses instead of a single event, the system goes through consecutive states of connection and disconnection between surface and groundwater. If the interval between pulses is increased, the aquifer has more time between pulses to transmit and redistribute the infiltrated water, the groundwater mound has more time to dissipate which increases the groundwater table depth under the river bed, and the unsaturated zone between surface and the water table has a lower moisture content when the next pulse occurs, leaving more storage available for future recharge. The percentage of the total flood volume that becomes recharge thus increases as shown in Fig 16 (right).

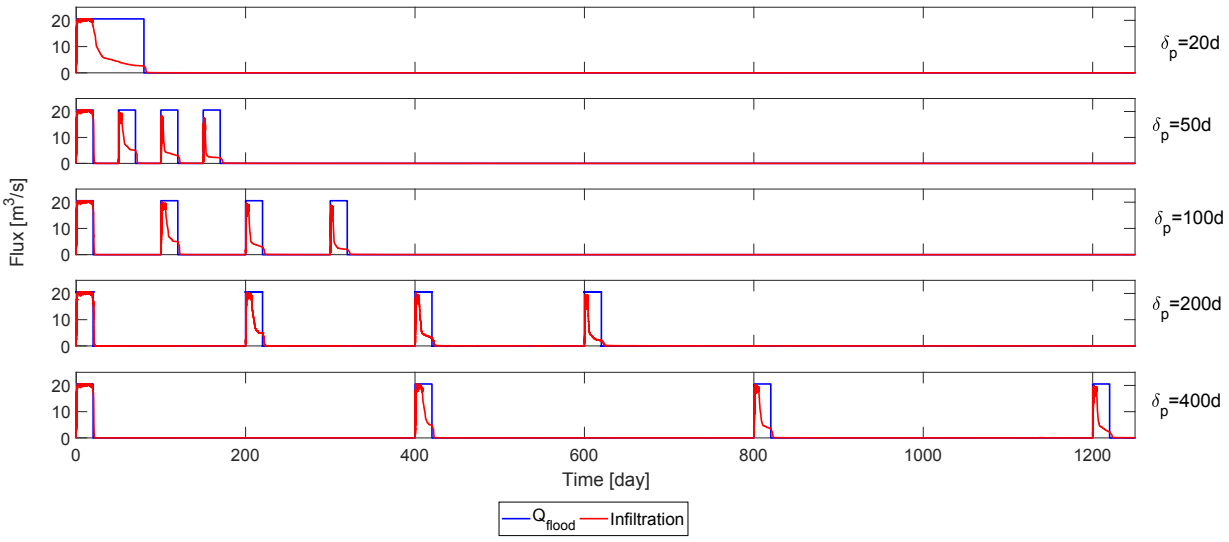

Figure 15: Temporal distributions of the flood volume in 4 pulses of 20 days and the resulting simulated infiltration. Pulses are released (δ_p) every 20 (no lag between pulses), 50, 100, 200 and 400 days.

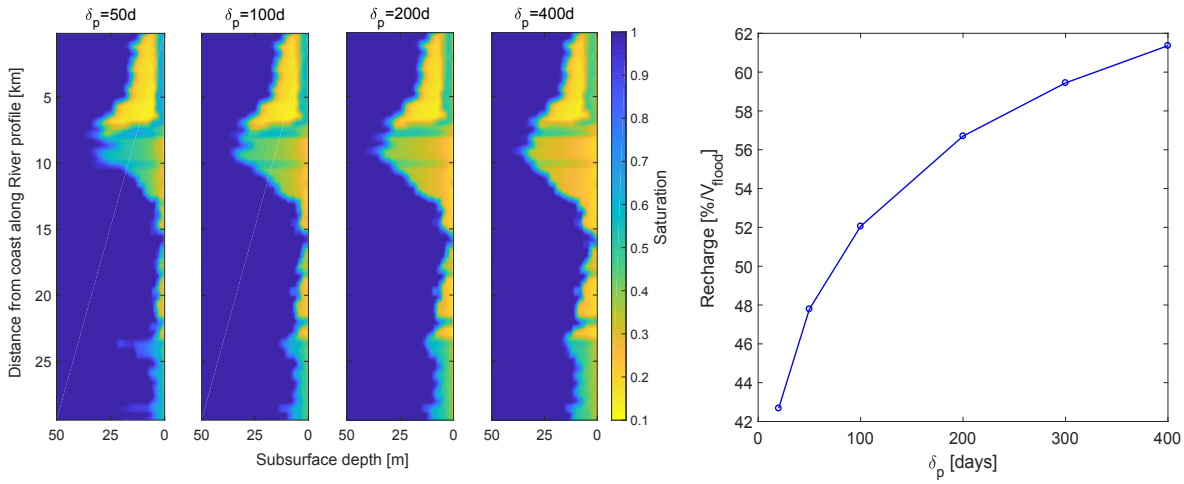

Figure 16: Vertical saturation profiles under the river bed just before the second pulse for the different temporal distributions of the total flood volume shown in Fig 15 [left]; and total recharge as percentage of the total flood volume for the different temporal distributions [right].

Discussion and Conclusions

We developed an integrated surface and subsurface hydrologic model to simulate recharge of an alluvial–fluvial aquifer during and after an extreme flooding event that occurred in 2001 in an arid valley in northern Chile. Although model structure and calibration were carried out using sparse knowledge about the area, the calibrated model provides a good representation of surface flow discharge and a reasonable estimation of groundwater table evolution with time at most observation locations, while calibrated parameters present reasonable values. Different factors may explain the mismatches between the observed and the simulated variables versus time.

The simulation of surface and groundwater, its distribution and resolution, and the water balance partitioning, depends on the assumptions and simplifications made about the geometry of the surface and subsurface domains, the representation of river sections, flood plains topography and microtopography, the stream bed and aquifer heterogeneities, and human and natural processes. These factors potentially control surface and subsurface water redistribution, river–aquifer water exchange and the local transient behavior of the infiltrated water specially when the water table is deep (Tayfur et al., 1993; Frei et al., 2009; Caviedes-Voullième et al., 2012). Neglecting pumping activity, especially near observation wells, could explain some of the discrepancies between observed and simulated hydraulic heads. The cumulative effect of previous flooding events and percolation from irrigation imposes an initial soil moisture condition that will result in a reduction of infiltrated water over stream channels and irrigated flood plains. Also, soil moisture is relevant to determine evapotranspiration, which has not been explicitly considered here. Evapotranspiration from riparian vegetation and agricultural behavior sometimes may have a considerable effect on percolation rates (Blasch et al., 2004). Recharge to the deeper regional aquifer would not occur for shorter

floodings due to evapotranspiration. On the other hand, evaporation becomes less important for larger flow events but increases if there are low permeability layers beneath the stream Shanafield and Cook (2014). Intensive floods in arid regions produce soil erosion, leading to increasing loading of sediments that settle in low velocity areas and form clogging layers. These effects and the influence of subsurface materials heterogeneities on infiltration have been studied for example by Brunner et al. (2009b); Sciuto and Diekkrüger (2010); Doble et al. (2011); Irvine et al. (2012).

Simulating coupled surface and subsurface flow allowed to spatially assess the relation between surface runoff, infiltration capacity, soil moisture and groundwater table depth that define the main system recharge at every time during and after the flooding event. Accounting for variably-saturated flow has also been shown to be critical to simulate recharge induced by surface flow events.

Three different infiltration rate behaviors are distinguished during the flood event. First, there is a short transient period with larger infiltration rates due to the high matric potential of the shallow unsaturated soils. Then, when soil moisture increases, gravity becomes dominant and infiltration reaches a steady-state value limited by the saturated hydraulic conductivity of the shallow soil layers. A saturated wetting front progressively advances downward with time, through the vadose zone. When flood conditions persist, the surface and groundwater systems connect and direct recharge to the groundwater table begins, infiltration rates decrease considerably as a result of the limited capacity of the aquifer to redistribute the infiltrated water out of the flooded areas.

For the calibrated model, the time when connection between surface and ground water occurs and infiltration rates decrease depends mainly on the antecedent soil moisture in the unsaturated zone and the initial water table depth. Water that infiltrates but does not reach the water table remains in the unsaturated zone and is thus available to contribute to groundwater recharge for future events. On the other hand, water that infiltrates in flood plains in non–active flowing areas may never contribute to recharge but can have an important effect on downstream flow discharge.

One of the main conclusions derived from the results of the simulations, which is consistent with the results of previous studies (Shentsis and Rosenthal, 2003; Taylor et al., 2013; Bartsch et al., 2014, e.g.), is that total recharge could be enhanced during flood events with a proper management of extractions and groundwater levels. The total recharged volume is quasi-linearly dependent on the initial water table depth in the aquifer. The simulation of different flood pulses distributed in time showed how consecutive flooding events impact on total infiltration, recharge and surface flow depending on antecedent conditions. Total infiltration would increase if the water volume that flows through the valley during occasional floods could be regulated. Furthermore, we verified that infiltration that significantly contributes to recharge takes place along the main flow channel, and other higher stage channels and plains with active flow during flooding. Thus, the flood duration is more important than flood stage and hydrograph shape when the latter not produces significant variation in active flooding areas. Then, it could be possible to enhance total recharge by increasing the active flowing areas by, for example, reconnecting side channels, terraces and flood plains.

Based on the results and comments above we conclude on some potential future improvements to this research and for the future development of models to predict recharge.

The impact of using a more detailed representation of hydraulic conductivity heterogeneities and a higher resolution topography to define the river channel and flooded plains on the simulated surface flow, flooded areas extension and local transient behavior of groundwater table ascensions, should be examined. Using locally refined meshes would allow to simulate the surface–subsurface flux exchange process with better resolution and calibrated parameters more representative of smaller scale values, at the expense of larger computational efforts (Doble et al., 2011, 2012; Caviedes-Voullième et al., 2012).

Measurements of surface flow discharge at the upper and intermediate sections of the valley would be useful to more accurately estimate transmission losses between different sections and improve the calibration of surface and subsurface parameters. The use of traditional measurement techniques is difficult due to the extreme conditions of stream flows. Additional information about flooded areas and surface flow obtained through indirect techniques, such as surface water level marks measurements, photo or video images, and satellite radar imagery data, would be useful to improve model calibration (Muste et al., 2008; Di Baldassarre et al., 2009).

A better understanding of the impact of the initial conditions assumed in the model to simulate intense flood event would help to minimize the influence of the initial state of the model, to avoid the exclusion of initial model outputs (especially when information is limited) and also to assure and facilitate the course of the numerical simulation (Rahman and Lu, 2015). The infiltration response of the subsurface system to the extreme surface flow, the connection of surface and subsurface systems, and the total recharge are highly dependent on antecedent conditions. Previous data of pumping and irrigation activities, evapotranspiration and past flood events, and measurements of soil moisture content and groundwater table depths are needed to study and perform an appropriate approach to determine initial conditions for the parameterized model (Berthet et al., 2009; Ajami et al., 2014), especially for a variably-saturated subsurface domain. Moreover, further work is necessary to understand and quantify the effect of the different hydrological processes and anthropic stresses on flood water infiltration, groundwater recharge and discharge, and water balance, for a wide range of scales and hydrogeological systems.

We demonstrated that, even with limited data, an integrated surface and subsurface hydrologic model can simulate extreme flood–recharge process at the watershed scale in arid environments and provide physically plausible results. We used the model as a tool to increase the understanding of infiltration mechanisms and recharge in the Valle de Azapa and to identify mechanisms and variables that control recharge. The simulation helped to assess the contribution of the surface flood to groundwater recharge under different parameters and initial states. The integrated surface and subsurface hydrologic model provides a promising alternative to evaluate integrated management strategies for aquifers and mitigation solutions for extreme climatic events. Furthermore, we expect that the new knowledge generated with this study can translate to other arid regions around the world.

Acknowledgments

The first and third authors acknowledge the financial support provided by the Center for Climate and Resilience Research (CR2), while the second author acknowledges support from the Natural Sciences and Engineering Research Council of Canada (NSERC). The first author is grateful for a travel grant awarded by the Universidad de Chile to be a visiting student at Université Laval.

Supplemental Material

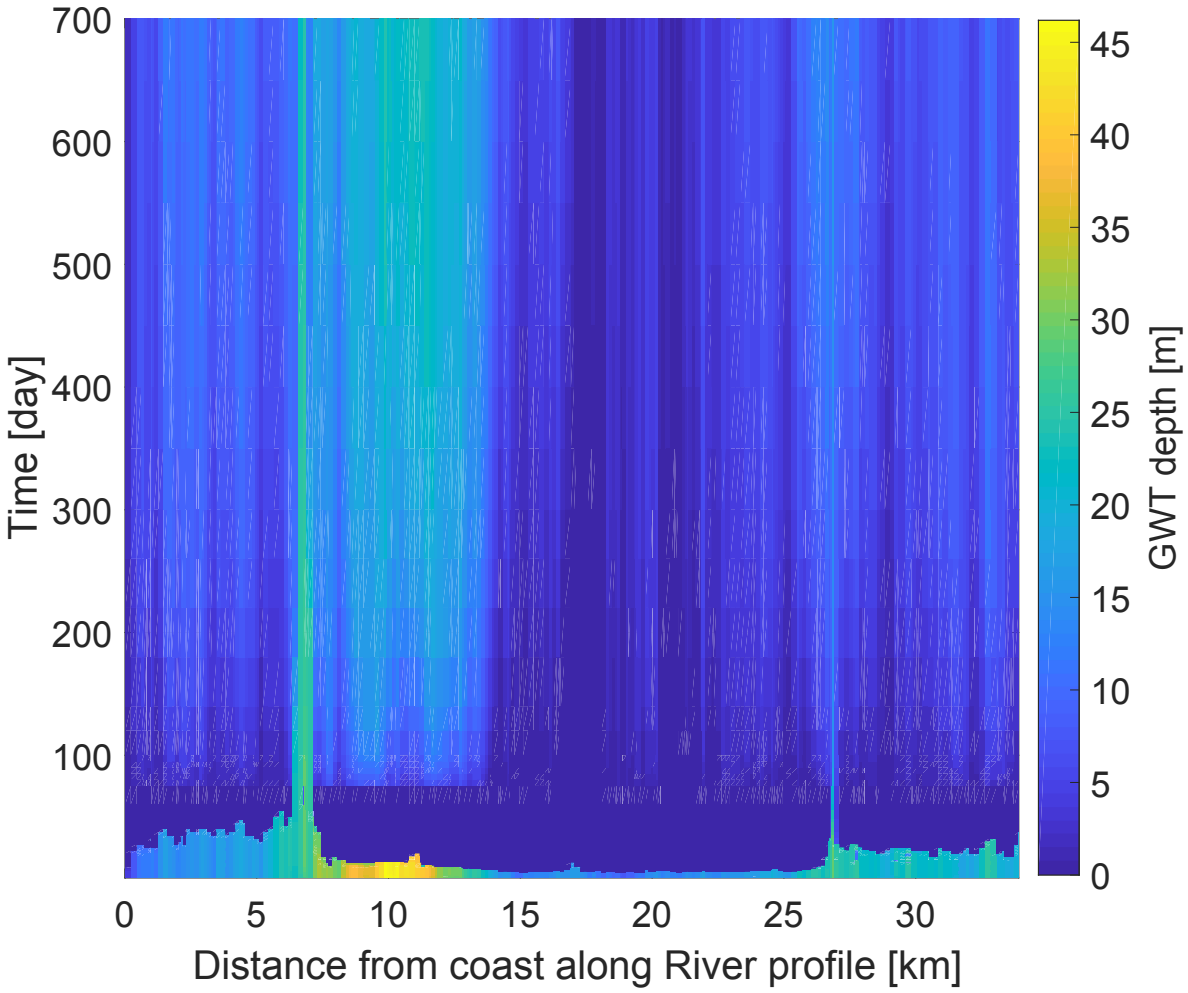

Figure S1: Groundwater table depth along the river longitudinal profile during the simulated time interval.

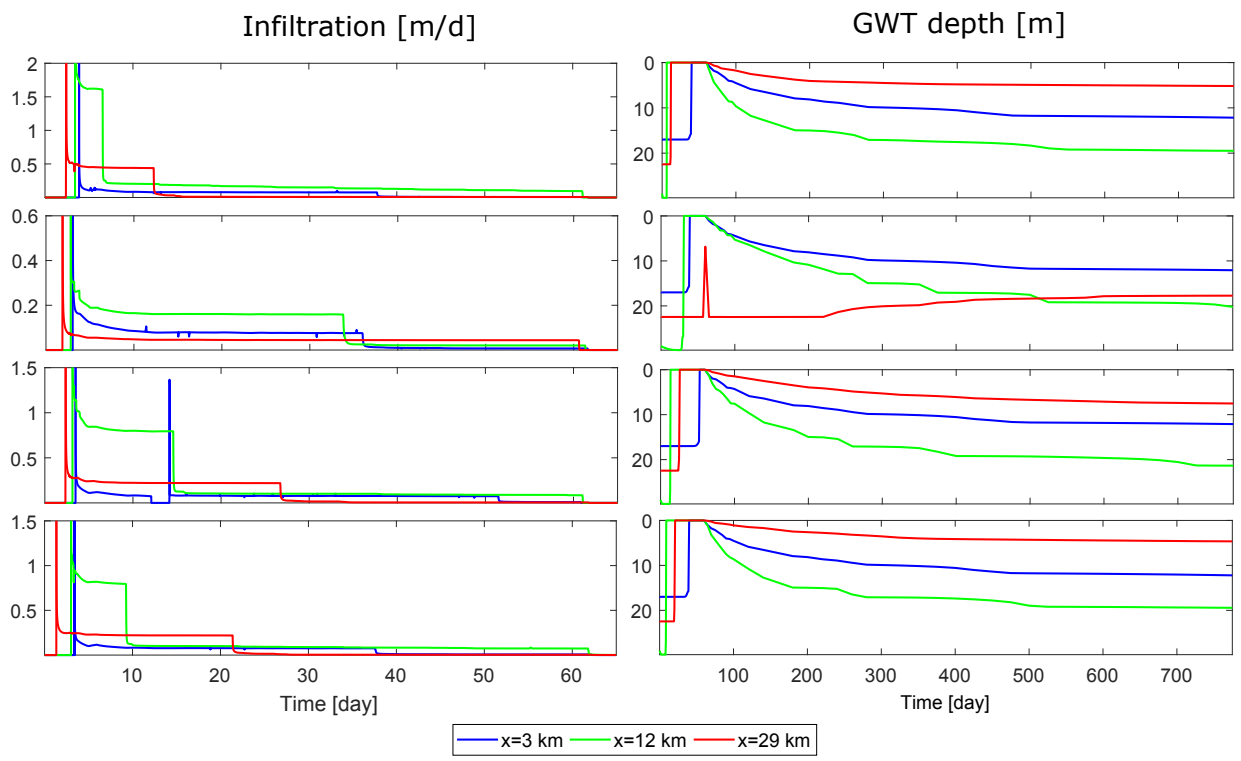

Figure S2: Infiltration rates during flooding event and GWT depth for the entire simulation at 3, 12 and 29 km from the coast along the longitudinal river profile of Fig4 , for the scenarios K1, K6, P3 and N2.

Conclusiones

Por medio de un modelo numérico integrado de flujo superficial y subterráneo del acuífero aluvial del Valle de Azapa se estudió el proceso de inundación, infiltración y recarga debido a una crecida extrema del río San José, permitiendo establecer relaciones entre nivel freático, humedad del suelo y capacidad de infiltración. Los resultados del modelo calibrado comparan razonablemente con los datos observados, reproduciendo el ascenso general del nivel freático en los pozos de observación y el caudal superficial en el tiempo para el evento simulado. Al mismo tiempo los parámetros calibrados que describen los medios superficial y subterráneo presentan valores dentro de lo esperado.

En particular, los valores calibrados de conductividad hidráulica son similares a los obtenidos por medio de pruebas de infiltración realizadas en estudios previos, donde se obtuvo una tasa de infiltración promedio para el largo plazo de 0.48 m/d (INH, 2014) considerando varios puntos distribuidos en el lecho y planicies de inundación del río. Estos valores son representativos de la conductividad hidráulica vertical de los suelos, la cual controla el proceso de infiltración. Si bien, se realizaron simulaciones considerando heterogeneidad y anisotropía de los suelos, se recomienda un estudio más profundo para incluir sus resultados, apoyado en caracterizaciones locales más precisas del subsuelo, para determinar los verdaderos efectos en la infiltración, percolación y redistribución de la recarga en el valle. Es común para este tipo de acuíferos que en profundidad se presente estratificación asociada a deposición de sedimentos de distintos eventos de inundación y otros procesos geológicos, así, verticalmente se pueden formar niveles saturados sobre estratos continuos o discontinuos de menor permeabilidad. Esto supone un retraso en la transformación de la percolación en recarga, simulada en el presente estudio por la definición de una conductividad hidráulica equivalente en la vertical. Sin embargo, en casos podría existir un encharcamiento temporal del suelo hasta la superficie, y el consecuente rechazo de la infiltración, o flujos preferenciales que determinen el comportamiento local de los ascensos observados.

La evaluación de la incertidumbre en el modelo conceptual y estructural escapa a los objetivos de esta tesis, sin embargo, es parte de la motivación para seguir explorando este tipo de modelación. La sensibilidad del sistema puede ser espacial y temporalmente identificada, y la incertidumbre reconocida y reducida con una evaluación de los supuestos realizados, con más información sobre el sistema, de los parámetros que lo caracterizan, y nuevas observaciones. Es fundamental evaluar directamente el efecto de la topografía, la discretización espacial y heterogeneidades del sistema, el efecto de las extracciones, la percolación del agua de riego y las perdidas evapotranspirativas.

El modelo es capaz de representar las variaciones temporales en las tasas de infiltración debido a los cambios de gradiente hidráulico en la interfaz agua sedimento. Inicialmente se producen altas tasas de infiltración debido a un gradiente hidráulico alto generado por una rápida subida de los niveles de agua superficial y el alto potencial de succión de los suelos secos. Si la inundación persiste, el suelo rápidamente se satura, se tiende a un gradiente hidráulico unitario en la interfaz agua sedimento y la gravedad controla el proceso de avance en profundidad del agua infiltrada a una tasa casi constante, limitada por la conductividad hidráulica saturada del suelo. Cuando el frente de humedad alcanza el nivel freático y se

transmite la carga hidráulica a la superficie, el gradiente hidráulico en la interfaz disminuye, y la infiltración se ve limitada por la capacidad del acuífero (su geometría y estructura) de mover el agua infiltrada fuera de la zona de inundación.

Al considerar condiciones variables de humedad y simular el flujo de agua en la zona no saturada del suelo, el modelo permite la distinción temporal entre agua infiltrada y el agua que alcanza el nivel freático y constituye la recarga. Los resultados obtenidos indican que un 41.2 % de los 1.42E+08 m^3 de la crecida calibrada para el año 2001 en Ausipar se recargan al acuífero luego de dos años, mientras que un 5.4 % queda retenido en la zona no saturada. Considerando que la precipitación total durante el evento de crecida fue de aproximadamente 290 mm en la cuenca alta del río San José, se estima un volumen precipitado de 2.32E+08 m^3, con lo que un 60 % de este volumen correspondería a la crecida estimada en Ausipar y un 25 % a la recarga del acuífero aluvial del Valle de Azapa.

El valor de recarga estimado debido a la crecida concuerda con estimaciones anteriores (AC, 2010), donde la recarga durante el año 2001 y 2002, la cual estaría determinada principalmente por la crecida del año 2001, se estimó en aproximadamente 6E+07 m^3. Por otro lado, estudios anteriores (Ayala, 1989) desarrollados a partir de mediciones puntuales de caudal efectuadas simultáneamente en la estación San José antes bocatoma Azapa (Q1) (inmediatamente aguas abajo de Ausipar) y en San José en puente Saucache (Q2), proponen la siguiente relación de caudales para crecidas del rio San José: $Q2 = 500 + 0{,}52 * Q1$ [l/s]. Para caudales altos (10<Q1 m^3/s) esta relación indica que aproximadamente un 48 % del caudal Q1 se infiltra entre ambas estaciones, lo cual concuerda con la estimación de caudal calibrado en el presente estudio para los tiempos en que el sistema superficial se encuentra desconectado del subterráneo y ocurre la mayor infiltración.

Se verificó que la infiltración es cuasi linealmente dependiente de la profundidad inicial del nivel freático y que, junto al contenido antecedente de humedad de los suelos, controla cuando ocurre la conexión entre los sistemas superficial y subterráneo y el tiempo en que disminuyen considerablemente las tasas de infiltración. La diferencia entre infiltración y recarga aumenta para niveles freáticos iniciales más profundos, debido a que el agua infiltrada queda retenida en una zona no saturada de mayor espesor. Así, las condiciones iniciales son determinantes al momento de estimar la recarga, ya que junto a la estructura del suelo, controlan el tiempo y volumen disponible de recarga.

Los resultados de las simulaciones indican que la infiltración y recarga se relaciona de manera directa con la extensión y tiempo de inundación persistente mientras el sistema superficial se encuentre desconectado hidráulicamente del subterráneo. Localmente, al saturarse las primeras capas de suelo, variaciones de la altura de agua no afectan la infiltración, dado que se mantiene un gradiente hidráulico unitario en la interfaz, controlando la conductividad hidráulica saturada del suelo. Luego, la topografía y microtopografía superficial son fundamentales al momento de definir zonas preferenciales de flujo, las cuales deberían contrastarse con mediciones y observaciones (p ej. imágenes satelitales, alturas de escurrimiento, etc.) para mejorar la calibración de los parámetros que caracterizan el medio superficial y subterráneo.

Por otro lado, una distribución discontinua de un volumen determinado de crecida en distintos eventos separados temporalmente, permite generar una desconexión hidráulica entre el agua superficial y subsuperficial entre cada evento, lo que se traduce en condiciones ante-

cedentes de humedad en la zona no saturada y un nivel freático para los eventos siguientes que favorecen la recarga total al acuífero. Así, una regulación de las crecidas, por ejemplo mediante la construcción de embalses, permitiría aumentar la recarga del sistema.

En cuanto a los tiempos de simulación, estos dependen de las características de los procesos simulados, las variaciones y evolución de las variables de estado. Conocer el desarrollo de la solución espacial y temporal permite mejorar aspectos de la malla, configurar los criterios de convergencia y los parámetros de control de ejecución durante la simulación para optimizar los tiempos de ejecución. El modelo calibrado, luego de optimizar su ejecución demora aproximadamente 5.5 horas de CPU en correr los 700 días de simulación utilizando un PC HP Elitedesk 800 G1 SFF y paralelizando en 6 núcleos. Debido a los gradientes altos de presión producidos inicialmente durante la crecida, para los primeros 50 días se resuelve a un paso de tiempo pequeño (0.01 días en promedio) para asegurar la convergencia de la solución. Luego el paso de tiempo aumenta linealmente hasta alcanzar un valor de 11 días al final de la simulación.

Finalmente, se concluye que la aplicación de HGS para el estudio de un evento de crecida en el Valle de Azapa, confirmó la viabilidad de utilizar este tipo de modelos para mejorar el entendimiento del proceso de recarga por inundación. Se considera que el modelo desarrollado puede en primera instancia, considerando limitada información, ser utilizado para formular recomendaciones a futuras investigaciones, y guiar para optimizar la recolección de datos y observaciones. Como trabajo futuro, es fundamental evaluar directamente la incertidumbre asociada a la inclusión de los factores no considerados (por ej. extracciones, evapotranspiración, heterogeneidades, etc.), para lo cual modificaciones en la estructura y parametrización del modelo serían necesarias. Se considera que la modelación integrada y distribuida de procesos es una potente herramienta para el estudio de cambios de escala en hidrología y para encontrar un balance optimo y el complemento entre la aplicación de un enfoque interdisciplinario (complejidad) y uno basado en la reducción o simplificación de un sistema en particular.

Bibliografía

Abdalla, F., El Shamy, I., Bamousa, A., Mansour, A., Mohamed, A., and Tahoon, M. (2014). Flash floods and groundwater recharge potentials in arid land alluvial basins, southern Red Sea Coast, egypt. *International Journal of Geosciences*, 5(9):971.

AC, I. C. L. (2010). Definición de estrategias de manejo sustentable para el acuífero de Azapa, xv Región. Technical report, Directorate General of Water, Ministry of Public Works, The Republic of Chile.

Ajami, H., McCabe, M. F., Evans, J. P., and Stisen, S. (2014). Assessing the impact of model spin-up on surface water-groundwater interactions using an integrated hydrologic model. *Water Resources Research*, 50(3):2636–2656.

Andrew Maddocks, R. S. Y. and Paul Reig (2015). Ranking the World's Most Water-Stressed Countries in 2040. http://www.wri.org/blog/2015/08/ranking-world's-most-water-stressed-countries-2040.

Aquanty Inc, Waterloo, C. (2013). Hydrogeosphere user manual - release 1.0. *Manual*, 1.0.(1).

Arrau, L. (1997). Modelo de simulación hidrológico operacional cuenca del río San José. Technical report, Directorate General of Water, Ministry of Public Works, The Republic of Chile.

Ayala, C. y. A. L. (1989). Modelo de simulación de las aguas subterráneas del Valle de Azapa. Technical report, Directorate General of Water, Ministry of Public Works, The Republic of Chile.

Bartsch, S., Frei, S., Ruidisch, M., Shope, C. L., Peiffer, S., Kim, B., and Fleckenstein, J. H. (2014). River-aquifer exchange fluxes under monsoonal climate conditions. *Journal of Hydrology*, 509:601–614.

Berthet, L., Andréassian, V., Perrin, C., and Javelle, P. (2009). How crucial is it to account for the antecedent moisture conditions in flood forecasting? Comparison of event-based and continuous approaches on 178 catchments. *Hydrology and Earth System Sciences Discussions*, (13):p–819.

Besbes, M., Delhomme, J., and De Marsily, G. (1978). Estimating recharge from ephemeral streams in arid regions: a case study at Kairouan, Tunisia. *Water Resources Research*, 14(2):281–290.

Bethune, M., Selle, B., and Wang, Q. (2008). Understanding and predicting deep percolation under surface irrigation. *Water Resources Research*, 44(12).

Beven, K. (1995). Linking parameters across scales: Subgrid parameterizations and scale dependent hydrological models. *Hydrological Processes*, 9(5-6):507–525.

Bierkens, M. F., Bell, V. A., Burek, P., Chaney, N., Condon, L. E., David, C. H., de Roo, A., Döll, P., Drost, N., Famiglietti, J. S., et al. (2015). Hyper-resolution global hydrological modelling: What is next? Everywhere and locally relevant. *Hydrol Process*, 29(2):310–320.

Blasch, K., Ferré, T., Hoffmann, J., Pool, D., Bailey, M., and Cordova, J. (2004). Processes controlling recharge beneath ephemeral streams in southern Arizona. *Groundwater recharge in a desert environment: the Southwestern United States*, pages 69–76.

Blasch, K. W., Ferré, T., Hoffmann, J. P., and Fleming, J. B. (2006). Relative contributions of transient and steady state infiltration during ephemeral streamflow. *Water Resources Research*, 42(8).

Blöschl, G. and Sivapalan, M. (1995). Scale issues in hydrological modelling: A review. *Hydrological processes*, 9(3-4):251–290.

Bouwer, H. (2002). Artificial recharge of groundwater: Hydrogeology and engineering. *Hydrogeology Journal*, 10(1):121–142.

Bredehoeft, J. (2005). The conceptualization model problem-surprise. *Hydrogeology Journal*, 13(1):37–46.

Brunner, P., Cook, P. G., and Simmons, C. T. (2009a). Hydrogeologic controls on disconnection between surface water and groundwater. *Water Resources Research*, 45(1).

Brunner, P. and Simmons, C. T. (2012). Hydrogeosphere: a fully integrated, physically based hydrological model. *Groundwater*, 50(2):170–176.

Brunner, P., Simmons, C. T., and Cook, P. G. (2009b). Spatial and temporal aspects of the transition from connection to disconnection between rivers, lakes and groundwater. *Journal of Hydrology*, 376(1):159–169.

Caviedes-Voullième, D., García-Navarro, P., and Murillo, J. (2012). Influence of mesh structure on 2d full shallow water equations and SCS curve number simulation of rainfall/runoff events. *Journal of hydrology*, 448:39–59.

Cheng, L., Wang, Z., Hu, S., Wang, Y., Jin, J., and Zhou, Y. (2015). Flood routing model incorporating intensive streambed infiltration. *Science China Earth Sciences*, 58(5):718–726.

Cooley, R. L. (1971). A finite difference method for unsteady flow in variably saturated porous media: Application to a single pumping well. *Water Resources Research*, 7(6):1607–1625.

Cools, J., Vanderkimpen, P., El Afandi, G., Abdelkhalek, A., Fockedey, S., El Sammany, M., Abdallah, G., El Bihery, M., Bauwens, W., and Huygens, M. (2012). An early warning system for flash floods in hyper-arid Egypt. *Natural Hazards and Earth System Sciences*, 12(2):443–457.

Custodio, E., Llamas, M. R., and Samper, J. (1997). *La evaluación de la recarga a los acuíferos en la planificación hidrológica*. Asociación Internacional de Hidrogeólogos.

De Vries, J. J. and Simmers, I. (2002). Groundwater recharge: an overview of processes and challenges. *Hydrogeology Journal*, 10(1):5–17.

Di Baldassarre, G., Schumann, G., and Bates, P. D. (2009). A technique for the calibration of hydraulic models using uncertain satellite observations of flood extent. *Journal of Hydrology*, 367(3):276–282.

Doble, R., Crosbie, R., Smerdon, B., Peeters, L., Chan, F., Marinova, D., and Andersson, R. (2011). Examining the controls on overbank flood recharge for improved estimates of national water accounting.

Doble, R. C., Crosbie, R. S., Smerdon, B. D., Peeters, L., and Cook, F. J. (2012). Groundwater recharge from overbank floods. *Water Resources Research*, 48(9).

Ebel, B. A. and Loague, K. (2006). Physics-based hydrologic-response simulation: Seeing through the fog of equifinality. *Hydrological Processes*, 20(13):2887–2900.

Ebel, B. A., Mirus, B. B., Heppner, C. S., VanderKwaak, J. E., and Loague, K. (2009). First-order exchange coefficient coupling for simulating surface water–groundwater interactions: Parameter sensitivity and consistency with a physics-based approach. *Hydrological Processes*, 23(13):1949–1959.

El-Hames, A. and Richards, K. (1998). An integrated, physically based model for arid region flash flood prediction capable of simulating dynamic transmission loss. *Hydrological Processes*, 12(8):1219–1232.

Elfeki, A., Ewea, H., Bahrawi, J., and Al-Amri, N. (2015). Incorporating transmission losses in flash flood routing in ephemeral streams by using the three-parameter Muskingum method. *Arabian Journal of Geosciences*, 8(7):5153–5165.

Fatichi, S., Vivoni, E. R., Ogden, F. L., Ivanov, V. Y., Mirus, B., Gochis, D., Downer, C. W., Camporese, M., Davison, J. H., Ebel, B., et al. (2016). An overview of current applications, challenges, and future trends in distributed process-based models in hydrology. *Journal of Hydrology*, 537:45–60.

Finger, D., Pellicciotti, F., Konz, M., Rimkus, S., and Burlando, P. (2011). The value of glacier mass balance, satellite snow cover images, and hourly discharge for improving the performance of a physically based distributed hydrological model. *Water Resources Research*, 47(7).

Freeze, R. A. (1969). The mechanism of natural ground-water recharge and discharge: 1. One-dimensional, vertical, unsteady, unsaturated flow above a recharging or discharging ground-water flow system. *Water Resources Research*, 5(1):153–171.

Freeze, R. A. and Harlan, R. (1969). Blueprint for a physically-based, digitally-simulated hydrologic response model. *Journal of Hydrology*, 9(3):237–258.

Frei, S., Fleckenstein, J., Kollet, S., and Maxwell, R. (2009). Patterns and dynamics of river–aquifer exchange with variably-saturated flow using a fully-coupled model. *Journal*

of Hydrology, 375(3):383–393.

Garreaud, R. (2011). Cambio climático: Bases físicas e impactos en chile. *Revista Tierra Adentro - INIA*, (93).

Gee, G. W. and Hillel, D. (1988). Groundwater recharge in arid regions: review and critique of estimation methods. *Hydrological Processes*, 2(3):255–266.

Green, T. R., Taniguchi, M., Kooi, H., Gurdak, J. J., Allen, D. M., Hiscock, K. M., Treidel, H., and Aureli, A. (2011). Beneath the surface of global change: Impacts of climate change on groundwater. *Journal of Hydrology*, 405(3):532–560.

Guthke, A. (2017). Defensible model complexity: A call for data-based and goal-oriented model choice. *Groundwater*, 55(5):646–650.

H. Peña, C. S. y. A. P. (1995). Estudio del origen de salinización de las aguas subterráneas en el Valle de Azapa. i Región, Chile. Technical report, Directorate General of Water, Ministry of Public Works, The Republic of Chile.

Hassan, S. (2011). Impact of flash floods on the hydrogeological aquifer system at Delta Wadi El-Arish (North Sina). In *Fifteenth International Water Technology Conference, IWTC*, volume 15, pages 28–30.

Healy, R. W. (2010). *Estimating groundwater recharge*. Cambridge University Press.

Houston, J. (2006a). The great Atacama flood of 2001 and its implications for Andean hydrology. *Hydrological Processes*, 20(3):591–610.

Houston, J. (2006b). Variability of precipitation in the Atacama Desert: its causes and hydrological impact. *International Journal of Climatology*, 26(15):2181–2198.

INH, I. N. H. (2014). Caracterización de la cuenca del río San José para la implementación de un programa de recarga artificial de acuíferos. Technical report, National Hydraulic Institute, Ministry of Public Works, The Republic of Chile.

Irvine, D. J., Brunner, P., Franssen, H.-J. H., and Simmons, C. T. (2012). Heterogeneous or homogeneous? Implications of simplifying heterogeneous streambeds in models of losing streams. *Journal of Hydrology*, 424:16–23.

JICA, J. I. C. A. (1995). The study on the development of water resources in Northern Chile. Technical report, Directorate General of Water, Ministry of Public Works, The Republic of Chile.

Jiménez Martínez, G. E. (2013). Caracterización de la cuenca del río San José en Arica para la evaluación a nivel de perfil de un sistema de recarga artificial de acuíferos.

Khu, S.-T., Madsen, H., and Di Pierro, F. (2008). Incorporating multiple observations for distributed hydrologic model calibration: An approach using a multi-objective evolutionary algorithm and clustering. *Advances in Water Resources*, 31(10):1387–1398.

Kinzelbach, W., Aeschbach, W., Alberich, C., Goni, I., Beyerle, U., Brunner, P., Chiang, W., Rueedi, J., and Zoellmann, K. (2002). A survey of methods for groundwater recharge in arid and semi-arid regions. *Early warning and assessment Report series, UNEP/DEWA/RS*, 2(2).

Koster, R. D. and Suarez, M. J. (2001). Soil moisture memory in climate models. *Journal of hydrometeorology*, 2(6):558–570.

Letniowski, F. and Forsyth, P. A. (1991). A control volume finite element method for three-dimensional NAPL groundwater contamination. *International Journal for Numerical Methods in Fluids*, 13(8):955–970.

Lilliefors, H. W. (1967). On the Kolmogorov-Smirnov test for normality with mean and variance unknown. *Journal of the American Statistical Association*, 62(318):399–402.

Maxwell, R. M., Putti, M., Meyerhoff, S., Delfs, J.-O., Ferguson, I. M., Ivanov, V., Kim, J., Kolditz, O., Kollet, S. J., Kumar, M., et al. (2014). Surface-subsurface model intercomparison: A first set of benchmark results to diagnose integrated hydrology and feedbacks. *Water Resources Research*, 50(2):1531–1549.

McCabe, M. F., Rodell, M., Alsdorf, D. E., Miralles, D. G., Uijlenhoet, R., Wagner, W., Lucieer, A., Houborg, R., Verhoest, N. E., Franz, T. E., et al. (2017). The future of earth observation in hydrology. *Hydrology and Earth System Sciences*, 21(7):3879.

Morin, E., Grodek, T., Dahan, O., Benito, G., Kulls, C., Jacoby, Y., Van Langenhove, G., Seely, M., and Enzel, Y. (2009). Flood routing and alluvial aquifer recharge along the ephemeral arid Kuiseb River, Namibia. *Journal of Hydrology*, 368(1):262–275.

Mualem, Y. (1976). A new model for predicting the hydraulic conductivity of unsaturated porous media. *Water Resources Research*, 12(3):513–522.

Muste, M., Fujita, I., and Hauet, A. (2008). Large-scale particle image velocimetry for measurements in riverine environments. *Water Resources Research*, 44(4).

Panday, S. and Huyakorn, P. S. (2004). A fully coupled physically-based spatially-distributed model for evaluating surface/subsurface flow. *Advances in Water Resources*, 27(4):361–382.

Paniconi, C. and Putti, M. (2015). Physically based modeling in catchment hydrology at 50: Survey and outlook. *Water Resources Research*, 51(9):7090–7129.

Park, Y.-J., Sudicky, E. A., Panday, S., and Matanga, G. (2009). Implicit subtime stepping for solving nonlinear flow equations in an integrated surface–subsurface system. *Vadose Zone Journal*, 8(4):825–836.

Peña H., Salazar C., P. A. (1994). Study of the origin and salinization processes of groundwater en the Azapa Valley, I Region. Chile. *Isotope hydrology investigations in Latin America 1994*, pages 91–105.

Philipp, A. and Grundmann, J. (2013). Integrated modeling system for flash flood routing in

ephemeral rivers under the influence of groundwater recharge dams. *Journal of Hydraulic Engineering*, 139(12):1234–1246.

Rahman, M. M. and Lu, M. (2015). Model spin-up behavior for wet and dry basins: a case study using the Xinanjiang model. *Water*, 7(8):4256–4273.

Scanlon, B. R., Healy, R. W., and Cook, P. G. (2002). Choosing appropriate techniques for quantifying groundwater recharge. *Hydrogeology Journal*, 10(1):18–39.

Scanlon, B. R., Keese, K. E., Flint, A. L., Flint, L. E., Gaye, C. B., Edmunds, W. M., and Simmers, I. (2006). Global synthesis of groundwater recharge in semiarid and arid regions. *Hydrological Processes*, 20(15):3335–3370.

Sciuto, G. and Diekkrüger, B. (2010). Influence of soil heterogeneity and spatial discretization on catchment water balance modeling. *Vadose Zone Journal*, 9(4):955–969.

Sellars, S., Nguyen, P., Chu, W., Gao, X., Hsu, K.-l., and Sorooshian, S. (2013). Computational earth science: Big data transformed into insight. *Eos, Transactions American Geophysical Union*, 94(32):277–278.

Shanafield, M. and Cook, P. G. (2014). Transmission losses, infiltration and groundwater recharge through ephemeral and intermittent streambeds: A review of applied methods. *Journal of Hydrology*, 511:518–529.

Shentsis, I. and Rosenthal, E. (2003). Recharge of aquifers by flood events in an arid region. *Hydrological Processes*, 17(4):695–712.

Simmers, I. (1998). Groundwater recharge: an overview of estimation 'problems' and recent developments. *Geological Society, London, Special Publications*, 130(1):107–115.

Simmers, I., Hendrickx, J., Kruseman, G., and Rushton, K. (1997). *Recharge of phreatic aquifers in (semi-) arid areas*. AA Balkema Rotterdam.

Sophocleous, M. (2002). Interactions between groundwater and surface water: the state of the science. *Hydrogeology Journal*, 10(1):52–67.

Sorman, A. U. and Abdulrazzak, M. J. (1993). Infiltration-recharge through wadi beds in arid regions. *Hydrological Sciences Journal*, 38(3):173–186.

Tayfur, G., Kavvas, M. L., Govindaraju, R. S., and Storm, D. E. (1993). Applicability of st. venant equations for two-dimensional overland flows over rough infiltrating surfaces. *Journal of Hydraulic Engineering*, 119(1):51–63.

Taylor, G. C. (1949). Geology and ground water of the azapa valley, province of tarapaca, chile. *Economic Geology*, 44(1):40–62.

Taylor, R. G., Scanlon, B., Döll, P., Rodell, M., Van Beek, R., Wada, Y., Longuevergne, L., Leblanc, M., Famiglietti, J. S., Edmunds, M., et al. (2013). Ground water and climate change. *Nature Climate Change*, 3(4):322–329.

Therrien, R., McLaren, R., Sudicky, E., and Panday, S. (2010). Hydrogeosphere: a three-dimensional numerical model describing fully-integrated subsurface and surface flow and solute transport. *Groundwater Simulations Group, University of Waterloo, Waterloo, ON*.

Therrien, R. and Sudicky, E. (1996). Three-dimensional analysis of variably-saturated flow and solute transport in discretely-fractured porous media. *Journal of Contaminant Hydrology*, 23(1-2):1–44.

Valdés-Pineda, R., Pizarro, R., García-Chevesich, P., Valdés, J. B., Olivares, C., Vera, M., Balocchi, F., Pérez, F., Vallejos, C., Fuentes, R., et al. (2014). Water governance in chile: Availability, management and climate change. *Journal of Hydrology*, 519:2538–2567.

Van Genuchten, M. T. (1980). A closed-form equation for predicting the hydraulic conductivity of unsaturated soils. *Soil Science Society of America Journal*, 44(5):892–898.

Western, A. W., Grayson, R. B., and Blöschl, G. (2002). Scaling of soil moisture: A hydrologic perspective. *Annual Review of Earth and Planetary Sciences*, 30(1):149–180.

Winter, T. C. (1995). Recent advances in understanding the interaction of groundwater and surface water. *Reviews of Geophysics*, 33(S2):985–994.

Xie, Y., Cook, P. G., Brunner, P., Irvine, D. J., and Simmons, C. T. (2014). When can inverted water tables occur beneath streams? *Groundwater*, 52(5):769–774.